

Geochronology and geochemistry of the Paleoproterozoic Fangniushan supracrustal strata in the Xiaoshan area, southern North China Craton: Implications for tectonic evolution



Qianying Sun^{a,b}, Yanyan Zhou^c, Taiping Zhao^{a,*}, Lanyin Pang^{a,d}, Yifan Qiu^{a,d}

^a Key Laboratory of Mineralogy and Metallogeny, Guangzhou Institute of Geochemistry, Chinese Academy of Sciences, Guangzhou 510640, China

^b National-Regional Joint Engineering Research Center for Soil Pollution Control and Remediation in South China, Guangdong Key Laboratory of Integrated Agro-environmental Pollution Control and Management, Guangdong Institute of Eco-environmental Science & Technology, Guangdong Academy of Sciences, Guangzhou 510650, China

^c State Key Laboratory of Lithospheric Evolution, Institute of Geology and Geophysics, Chinese Academy of Sciences, Beijing 100029, China

^d University of Chinese Academy of Sciences, Beijing 100049, China

ARTICLE INFO

Keywords:

North China craton
Fangniushan metasedimentary rocks
Detrital zircon
Geochemistry
Tectonic evolution

ABSTRACT

The Fangniushan supracrustal strata located in Xiaoshan area is one of the best-preserved Paleoproterozoic lowgrade metasedimentary units exposed in the southern North China Craton, which is mainly composed of quartzite and feldspar quartzite with minor pebbly quartzite and conglomerates. It unconformably contacts with the underlying Taihua Complex and the overlying Paleoproterozoic Xiong'er Group. Ages of the youngest detrital zircons from the quartzites combined with the formation age of the overlying Xiong'er Group bracket the depositional time of the Fangniushan supracrustal strata at ca. 1.87–1.80 Ga. Low CIA (< 70), ICV (0.48–1.46) values and high $\text{SiO}_2/\text{Al}_2\text{O}_3$ (4.1–75.1) ratios for the Fangniushan metasedimentary rocks are suggestive of chemically mature source that experienced weak to moderate chemical weathering in their source areas, which is also supported by the A-CN-K signatures. Detrital zircon U-Pb ages of the Fangniushan metasedimentary rocks yield three populations of ~2.00 to 2.24 Ga, ~2.25 to 2.40 Ga and ~2.50 to 2.88 Ga. REE patterns combined with trace elements characteristics involving La, Th, Zr, Hf, Co and Sc reveal that the Fangniushan metasedimentary rocks dominantly received detritus from felsic sources in the Xiaoshan and adjacent Xiaoqinling, Xiong'ershan and Zhongtiaoshan areas. Taking all these geochronological and geochemical signatures into account, the Fangniushan supracrustal strata was most likely deposited in a retro-arc foreland setting. In combination with previous studies on other Paleoproterozoic metavolcanic-sedimentary sequences, we prefer that the southern NCC might have experienced tectonic regime change from rift to subduction during Paleoproterozoic.

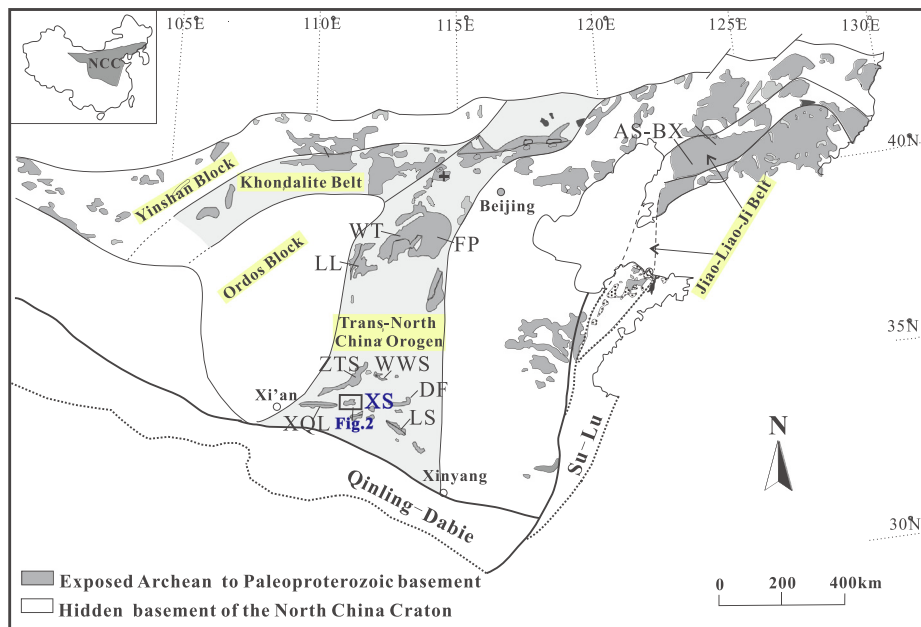
1. Introduction

The Neoarchean-Paleoproterozoic transition was marked by significant tectono-magmatic changes on Earth (e.g., Holland, 2002; Bekker et al., 2004; Lyons et al., 2014), which has witnessed the assembly of the Columbia or Nuna supercontinents in geological history. As one of the well-known oldest and largest cratons in the world (Liu et al., 1992), the North China Craton (NCC) has witnessed complicated early Precambrian evolutionary history. It is generally accepted that the different micro-continental blocks which constitute the NCC were closely related to the amalgamation of the Columbia supercontinent (Hou et al., 2008; Li et al., 2010a, 2012; Zhai and Santosh, 2011, 2013; Zhao et al., 2004a, 2011). However, it is still controversial on the number of

continental blocks, time and processes during the formation of the NCC in the reconstruction of the Columbia supercontinent (Zhai et al., 2000, 2005; Zhao et al., 2000, 2001, 2005; Kusky and Li, 2003; Kusky, 2011; Faure et al., 2007; Trap et al., 2012). A most popular view considered that the NCC can be divided into the Eastern and Western blocks, separated by the intervening Trans-North China Orogen (TNCO) (Fig. 1). One school of thought suggested that the final amalgamation of the NCC occurred at ~1.85 Ga by eastward subduction along the TNCO between the Eastern and Western blocks (Zhao et al., 2001, 2005, 2012b; Wilde et al., 2002; Kröner et al., 2005), whereas some other researchers proposed westward subduction with collision at ~2.5 Ga (Kusky et al., 2001; Kusky and Li, 2003; Polat et al., 2006) or westward subduction with two collisional events at ~2.1 Ga and ~1.85 Ga (Faure

* Corresponding author.

E-mail address: tpzhao@gig.ac.cn (T. Zhao).



et al., 2007; Trap et al., 2007, 2008, 2012). Therefore, the Paleoproterozoic tectonothermal events in the TNCO are vital importance for the overall evolution of the NCC.

The TNCO is a nearly NS-trending ~ 1200 km long and 100–300 km wide belt across the central part of the NCC. Based on the extensive structural, lithological, metamorphic, geochemical, and geochronological studies of the metamorphic complexes in the northern and central segments, Zhao et al. (2005, 2008) suggested that the TNCO may represent a long-lived magmatic arc (from 2.5 Ga to 1.85 Ga). However, although a number of studies focused on the Paleoproterozoic high-grade metamorphic and igneous rocks have been carried out in the past few years (e.g. Wan et al., 2006, 2013; Huang et al., 2012, 2013; Lu et al., 2013, 2014; Yu et al., 2013; Diwu et al., 2014; Zhou et al., 2014, 2015; Chen et al., 2016, 2020), it still remains unknown whether or not the southern segment of the TNCO also underwent such a long-lived subduction (Huang et al., 2013), which in turn, limits our understanding of the tectonic evolution of the TNCO as a whole in the Paleoproterozoic.

It is noteworthy that the final amalgamation and cratonicization of the NCC was traditionally considered to be related to the late Paleoproterozoic Lüliang Movement, which resulted in regional unconformity between Paleoproterozoic supracrustal strata and Mesoproterozoic sedimentary cover (Zhao et al., 1993). These Paleoproterozoic clastic sedimentary rocks, as geological records of the Archean-Paleoproterozoic tectonothermal events, can record valuable information of source rocks and provide rigorous constraints on the early crustal components and tectonic processes (Diwu et al., 2013; Wang et al., 2018a,b). Thus, geochronology and geochemistry studies of clastic sedimentary rocks have become one of the hotspots in geological research (e.g. Liu et al., 2016, 2018; Sun et al., 2017a,b). In the southern TNCO, Paleoproterozoic strata occur mainly in the Lushan, Dengfeng, Wangwushan, Zhongtiaoshan and Xiaoqinling areas, where from the east to west, the Upper Taihua, Songshan, Yinyugou, Zhongtiao, Danshanzi groups and Tietonggou Formation are exposed (Fig. 1). Recently, fewer studies have been done on depositional ages and environments of the Paleoproterozoic sedimentary sequences, but debate remains on the tectonic evolution process of them. For example, the Songshan Group in the Dengfeng Complex is tentatively correlated with the Hutuo Group in the Wutai Complex and both were interpreted to deposit in a rift basin (Du et al., 2009, 2010, 2017; Wan et al., 2009), whereas some researchers suggested that the lower part of the Hutuo

and Songshan groups were deposited after ~2.10 Ga and ~2.35 Ga, in accordance with collision between the Eastern and Western blocks along the TNCO at ~1.85 Ga (Liu et al., 2011, 2012a). Similar debates exist in interpreting the tectonic setting of the Upper Zhongtiao and Upper Taihua groups, which are thought to be formed either in foreland basins (Liu et al., 2012b) or in extensional continental setting (Sun et al., 1991; Geng et al., 2003, 2008; Sun et al., 2017b).

On the other hand, the Paleoproterozoic Fangniushan supracrustal strata outcrops in the Xiaoshan area of the southern NCC, in particular, is one of the best-preserved sedimentary sequences but is poorly studied by far. Low greenschist facies metamorphism of the sedimentary rocks imply little effect on the parent rocks, and thus the primary rock assemblages and geochemical compositions are well preserved. Besides, the Fangniushan supracrustal strata was unconformably overlies the Neoarchean Taihua Complex and overlain by the Mesoproterozoic Xiong'er Group, make it an ideal target to recognize the formation and tectonic evolution of the southern NCC from Neoarchean to Paleoproterozoic.

In this contribution, we present new field investigations, U-Pb-Hf isotopic compositions of detrital zircons, as well as whole-rock major and trace elements geochemistry of the Fangniushan metasedimentary rocks in the Xiaoshan area. Combined with other previously studies of sedimentary sequences in the southern NCC, the new dataset is used to investigate the depositional age, provenance and tectonic setting of the Fangniushan supracrustal strata, and further provide significant constraints on the Paleoproterozoic tectonic evolution of the southern NCC.

2. Geological background

The North China Craton (NCC), bounded by the Central Asian Orogenic Belt to the north and the Qinling-Dabie and Sulu Orogenic belts to the south (Fig. 1), is one of the oldest cratonic blocks in the world as old as 3.80 Ga (Liu et al., 2008; Wu et al., 2008; Zhai and Santosh, 2011; Zhai, 2014). Basement of the NCC is mainly composed of Neoarchean to Paleoproterozoic TTG gneisses, metamorphosed supracrustal units, and sparse Paleoarchean rocks, and is overlain by Mesoproterozoic to Cenozoic unmetamorphosed cover sequences (Zhao et al., 2012b). On the other hand, the Trans-North China Orogen (TNCO) in the prevailing model of Zhao et al. (2001) is mainly composed of Neoarchean to Paleoproterozoic TTG gneisses, syn- to post-tectonic granites and mafic dykes, meta-supracrustal rocks

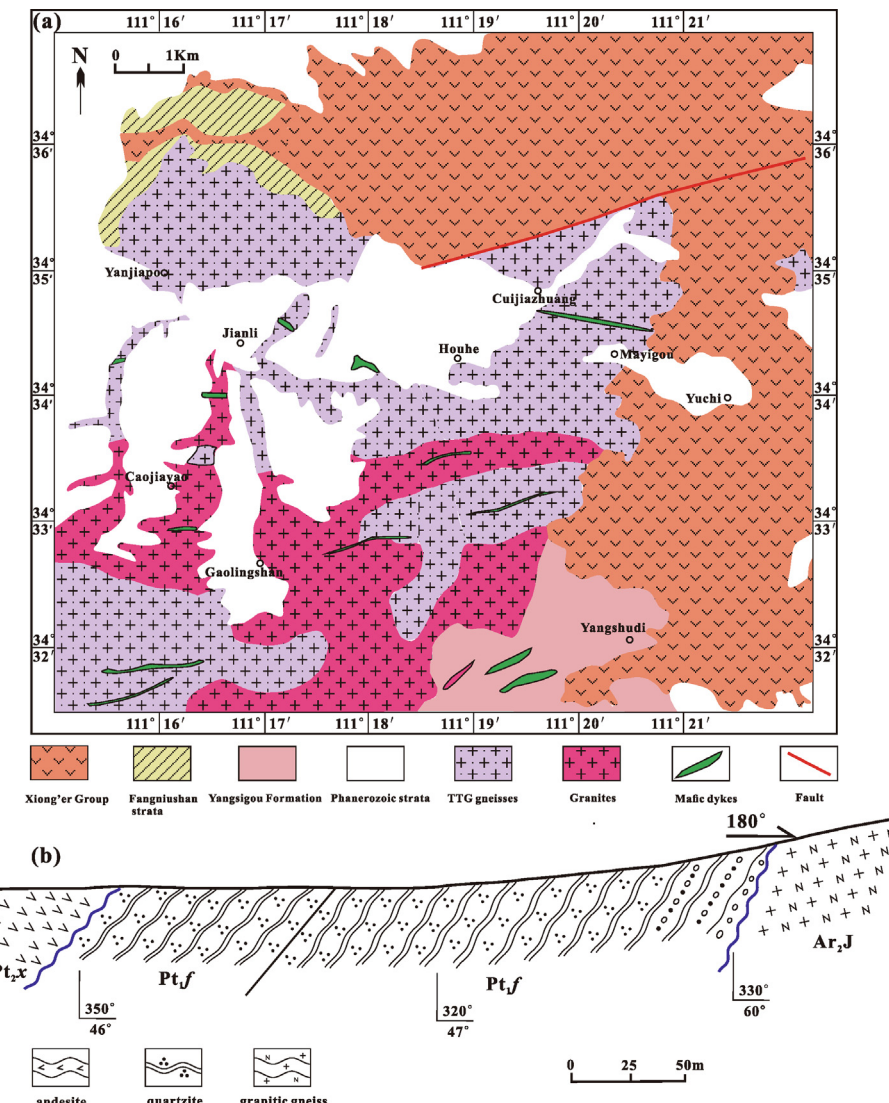


Fig. 2. (a). Simplified geological map of the Xiaoshan area (modified after BGMRHP, 1995). (b). A cross section through the Fangniushan supracrustal strata.

(metamorphic clastic sedimentary and volcanic rocks), as well as high-pressure granulites, retrograded eclogites and crustal-scale ductile shear zones (Zhao et al., 2001; Li et al., 2002; Kusky and Zhai, 2012).

The Fangniushan supracrustal strata outcrops in the Xiaoshan area, northwest of Henan Province, southern part of the TNCO. Early Precambrian successions in this area consist dominantly of Neoarchean to Paleoproterozoic Taihua Complex, Paleoproterozoic low-grade metamorphic supracrustal rock series, Mesoproterozoic Xiong'er, Guandaokou and Ruyang groups (Fig. 2a; 3) (Bureau of Geology and Mineral Resources of Henan Province (BGMRHP, 1995).

The Fangniushan supracrustal strata has been traditionally considered as part of the Songshan Group in the past (BGMRHP, 1995). However, based on detailed field mapping and regional comparison, we disagree with this view because of the following reasons: (1) The Fangniushan metasedimentary sequence overlies on the Taihua Complex of the Xiaoshan area and overlain by the Xiong'er Group with an angular unconformity (Fig. 2b; 3; 4a, b), while the Songshan Group overlies unconformably the Dengfeng Complex (Diwu et al., 2008; Liu et al., 2012a). (2) The ~500 m thick Fangniushan supracrustal strata is mainly composed of medium- to coarse-grained quartzite and feldspar quartzite in the lower part with minor pebbly quartzite and conglomerates in the upper part (Fig. 3), all of which have been metamorphosed in low greenschist facies. In addition, ripple marks and cross-bedding

structures still preserved in some quartzites (Fig. 4c, d), which was considered to have deposited in littoral sedimentary environment. However, the Songshan Group is a green-schist facies metamorphosed clastic-carbonate sedimentary strata dominantly consists of feldspar quartzites and mica schists, with interlayers of marble and carbonaceous schist (Diwu et al., 2008; Liu et al., 2012a). (3) The Fangniushan supracrustal strata was formed at late Paleoproterozoic, and dominantly received detritus from the early Paleoproterozoic crust (see our discussion below). Nevertheless, U-Pb ages of detrital zircons from the Songshan Group yielded age populations mainly at Meso-Neoarchean, with depositional age in the period between ~2.35 and ~1.80 Ga (Diwu et al., 2008; Liu et al., 2012a).

On the other hand, the Tietonggou Formation outcrops in the adjacent Xiaoqinling region consists of a succession of clastic sedimentary rocks, which unconformably overlies the Taihua Complex and overlain by the Xiong'er Group. The Fangniushan supracrustal strata show similar characteristics with the adjacent Tietonggou Formation in terms of lithologies (mainly quartzite and conglomerate), metamorphic grade (low greenschist facies), sedimentary environment (littoral facies terrigenous clastic formation), detrital zircon age distribution and depositional time (late Paleoproterozoic) (Diwu et al., 2013), thus, we uniformly regard them as the same strata deposited in different places.

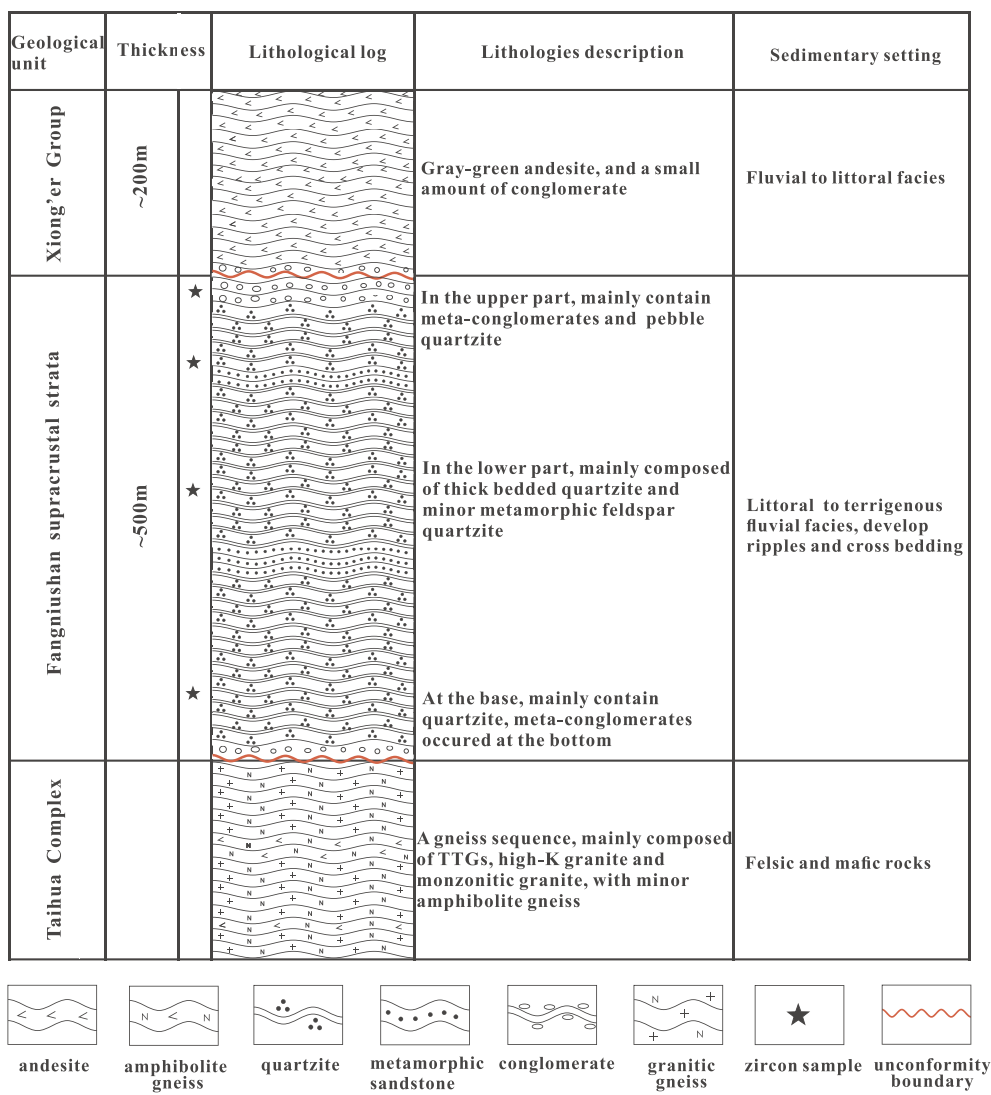


Fig. 3. Schematic stratigraphic section of Fangniushan supracrustal strata modified from BGMRHP (1995).

3. Samples and analytical methods

3.1. Zircon separation and CL imaging

Zircon grains were separated from three quartzite samples (17XS-5, 10, 19) and one feldspar quartzite sample (18XS-2) for zircon U-Pb dating and Hf isotope analysis. The sampling locations are shown in Fig. 3.

Zircon grains were separated using standard density and magnetic methods and then purified by hand-picked under a binocular microscope. The grains were randomly selected and were mounted in epoxy, then polished to expose half of the crystals for analysis. In order to reveal the origin and internal structure of zircon grains, Cathode-luminescence (CL) imaging was performed using a JXA-8100 Electron Probe Micro-analyzer with Mono CL3 cathode-luminescence System for high resolution imaging and spectroscopy at Guangzhou Institute of Geochemistry, Chinese Academy of Sciences (GIGCAS).

3.2. LA-ICP-MS zircon U-Pb dating

Zircon U-Pb dating was conducted at GIGCAS, using an Agilent 7500a ICP-MS combined with a Resonetics RESOlution M-50 (193 nm ArF excimer) laser ablation system. Helium was used as the carrier gas to enhance the transport efficiency of the ablated material. Laser

ablation was operated at a constant energy of 80 mJ at 8 Hz, with a spot diameter of 31 μm . The NIST SRM 610 and zircon 91,500 were used as the external calibration standards to calculate trace element concentrations and to normalize isotopic fractionation of unknowns, respectively. Each zircon grain analysis had a background acquisition time of ~20 s followed by sample data acquisition of 40 s. Detailed operating conditions and procedures are described by Li et al. (2015). U-Pb raw data were corrected offline using ICPMSDataCal (Liu et al., 2010), trace-element concentrations were obtained by normalizing count rates for each analyzed element to those for Zr to be stoichiometric in zircon. The age calculations and Concordia plots were made using Isoplot (version 3.0) (Ludwig, 2003). As a result of $^{207}\text{Pb}/^{206}\text{Pb}$ ages are more precise for older ages, we rely on $^{207}\text{Pb}/^{206}\text{Pb}$ ages as the zircon formation ages (Gehrels et al., 2006).

3.3. Zircon Hf isotope analysis

In situ zircon Lu-Hf isotopic analysis was performed using a Neptune MC-ICP-MS with a 193 nm laser ablation microprobe at GIGCAS. Detailed analytical procedure including instrument conditions and data acquisition are described in Xu et al. (2004) and Wu et al. (2006). A 44 μm laser diameter spot with a repetition rate of 8 Hz at laser power of 80 mJ/cm² were selected, resulting in 500 cycles data. Isobaric interference of ^{176}Yb on ^{176}Hf isotope was corrected using the intensity of

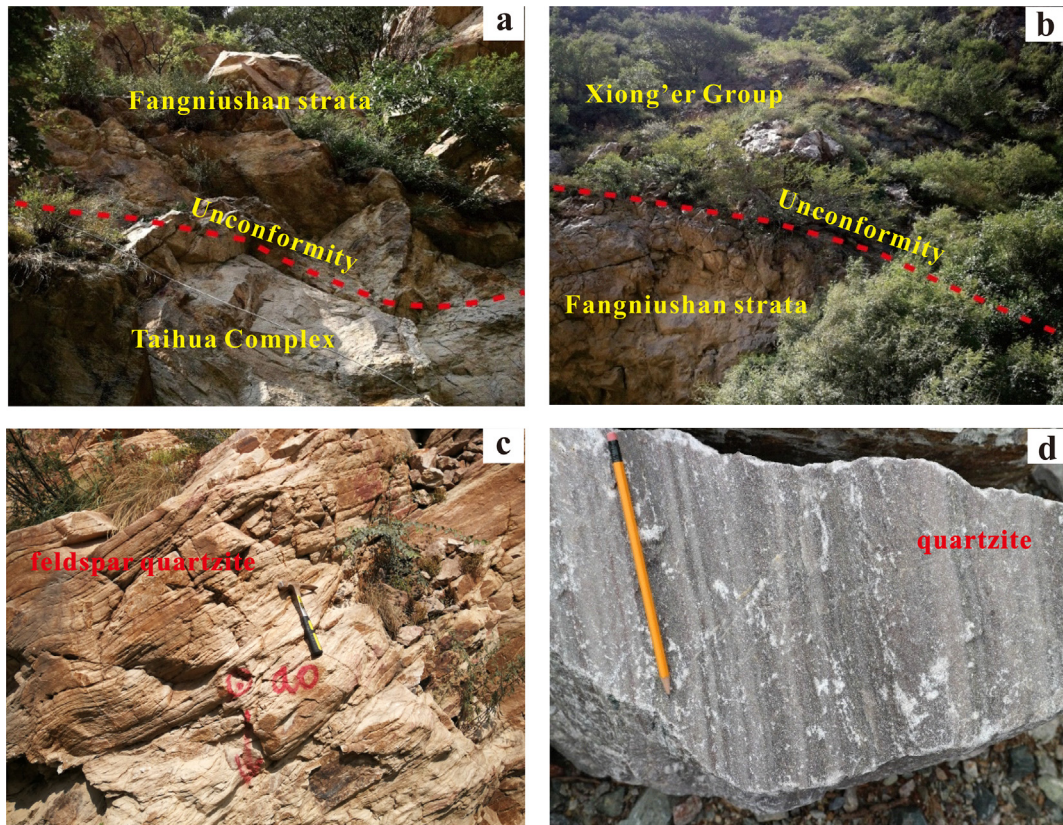


Fig. 4. Field relations of rocks from Fangniushan supracrustal strata (a) The boundary between the Fangniushan supracrustal strata and Taihua Complex. (b) The boundary between the Fangniushan supracrustal strata and Xiong'er Group. (c) Feldspar quartzite of the Fangniushan supracrustal strata. (d) Quartzite of the Fangniushan supracrustal strata.

the interference-free ^{172}Yb isotope and a recommended $^{176}\text{Yb}/^{172}\text{Yb}$ ratio of 0.5886 (Chu et al., 2002). Interference of ^{176}Lu on ^{176}Hf was corrected using the intensity of the interference-free ^{175}Lu isotope and a recommended $^{176}\text{Lu}/^{175}\text{Lu}$ ratio of 0.02655 (Machado and Siminetti, 2001). Zircon Penglai was used as the reference standard during routine analyses, with a recommended $^{176}\text{Hf}/^{177}\text{Hf}$ ratio of 0.282900 ± 50 (Li et al., 2010b). The present day chondritic ratios of $^{176}\text{Hf}/^{177}\text{Hf} = 0.282785$ and $^{176}\text{Lu}/^{177}\text{Hf} = 0.0336$ (Bouvier et al., 2008) were adopted to calculate $\varepsilon_{\text{Hf}}(t)$ values. Single-stage model ages (T_{DM1}) were calculated with respect to the depleted mantle with a present-day $^{176}\text{Hf}/^{177}\text{Hf}$ ratio of 0.28325 and $^{176}\text{Lu}/^{177}\text{Hf}$ ratio of 0.0384 (Griffin et al., 2000). Two-stage model ages (T_{DM2}) were calculated using a $^{176}\text{Lu}/^{177}\text{Hf}$ ratio (0.015) of the average continental crust derived from the depleted mantle (Griffin et al., 2002).

3.4. Whole-rock major and trace element analyses

Least-altered 15 (feldspar) quartzite samples were collected from the Fangniushan metasedimentary rocks for major and trace elements analyses at the GIGCAS. Samples were crushed and pulverized to powder of 200 mesh in agate mortars. Whole-rock major element analyses were performed by X-ray fluorescence spectrometry (XRF) on fused glass beads with the analytical uncertainties at $\pm 1\text{--}2\%$. The detailed analytical procedures were described in Li et al. (2006).

Trace elements, including REE, were analyzed using a Perkin-Elmer Scieix Elan 6000 inductively coupled plasma mass spectrometry (ICP-MS). Before analysis, the powdered samples (finer than 200 meshes) were digested with mixed acids of HNO_3 and HF acid in screw-top Teflon beakers for seven days at $\sim 100^\circ\text{C}$ to dissolve refractory minerals completely. Analytical procedures were similar to those described by Li (1997). A set of USGS and Chinese national rock standards, including

BHVO-2, GSR-1, GSR-2, GSR-3, AGV-2, W-2 and SARM-4, were chosen for calibration, with a precision better than 5% for most elements.

4. Results

4.1. Zircon U-Pb ages

LA-ICP-MS U-Pb analytical data are listed in Table 1 and reported as $^{207}\text{Pb}/^{206}\text{Pb}$ age, U-Pb results with discordance $> 10\%$ are thought to be unreliable and excluded out of consideration.

4.1.1. 17XS-5 (quartzite sample)

Zircons from the quartzite sample 17XS-5 are $80\text{--}200\ \mu\text{m}$ in length, with aspect ratios of 1:1–1:3 and prismatic or ellipsoidal in shape. CL images show that they have obvious oscillatory growth zonings (Fig. 5). These features, together with their high Th (40–559 ppm) and U (61–1064 ppm) contents and Th/U ratios (0.12–1.49, 0.63 on average), suggesting a magmatic origin (Vavra et al., 1999; Hoskin and Black, 2000). 85 analyzed spots acquired the concordant ages ranging from 1.83 to 2.83 Ga with a remarkable age peak at ~ 2.17 Ga and two sub peaks at ~ 2.31 Ga and ~ 2.47 Ga (Fig. 5). The youngest concordant zircon with concordance at 99% in this sample yields a $^{207}\text{Pb}/^{206}\text{Pb}$ age of 1833 ± 50 Ma.

4.1.2. 17XS-10 (quartzite sample)

In CL images (Fig. 5), zircon crystals from the quartzite sample 17XS-10 are typically subhedral-rounded or granular, and $50\text{--}220\ \mu\text{m}$ in length, with length/width ratios of 1:1–3:1. Most of the zircons contain oscillatory growth zoning and yield relatively high Th/U values (0.09–1.42, 0.67 on average) that indicate a magmatic origin (Vavra et al., 1999; Hoskin and Black, 2000). 74 analyses are concordant or

Table 1

LA-ICP-MS U-Pb dating results of zircons from the Fangniushan metasedimentary rocks in the Xiaoshan area.

Spot no.	Contents (ppm)		Th/U	Isotopic ratios						Age(Ma)						Concordance
	Th	U		$^{207}\text{Pb}/^{206}\text{Pb}$	1σ	$^{207}\text{Pb}/^{235}\text{U}$	1σ	$^{206}\text{Pb}/^{238}\text{U}$	1σ	$^{207}\text{Pb}/^{206}\text{Pb}$	1σ	$^{207}\text{Pb}/^{235}\text{U}$	1σ	$^{206}\text{Pb}/^{238}\text{U}$	1σ	
17XS-5																
1	184	365	0.50	0.1360	0.0016	7.4635	0.0974	0.3963	0.0034	2177	16	2169	12	2152	16	99%
2	65	78	0.84	0.1431	0.0018	8.4464	0.1296	0.4264	0.0045	2266	22	2280	14	2290	20	99%
3	154	233	0.66	0.1466	0.0015	8.6861	0.1011	0.4280	0.0035	2306	18	2306	11	2297	16	99%
4	144	218	0.66	0.1356	0.0015	7.4427	0.1012	0.3961	0.0039	2172	19	2166	12	2151	18	99%
5	100	185	0.54	0.1335	0.0015	7.6582	0.1060	0.4137	0.0041	2146	20	2192	13	2232	19	98%
6	96	148	0.65	0.1442	0.0018	8.6618	0.1275	0.4336	0.0045	2277	21	2303	13	2322	20	99%
7	95	188	0.50	0.1271	0.0016	7.0528	0.1050	0.4001	0.0039	2058	23	2118	13	2170	18	97%
8	78	128	0.60	0.1454	0.0021	8.9225	0.1436	0.4428	0.0047	2292	-8	2330	15	2363	21	98%
9	105	200	0.53	0.1322	0.0019	7.5928	0.1411	0.4136	0.0054	2127	26	2184	17	2231	25	97%
10	225	211	1.06	0.1325	0.0018	7.2384	0.1043	0.3940	0.0034	2131	23	2141	13	2141	16	99%
11	102	164	0.62	0.1317	0.0017	7.4622	0.1186	0.4084	0.0045	2121	23	2168	14	2208	21	98%
12	89	108	0.82	0.1439	0.0018	8.8501	0.1361	0.4450	0.0056	2276	21	2323	14	2373	25	97%
13	157	198	0.79	0.1599	0.0018	10.7110	0.1854	0.4828	0.0068	2455	19	2498	16	2539	30	98%
14	511	430	1.19	0.1415	0.0015	8.0536	0.1262	0.4103	0.0052	2246	19	2237	14	2216	24	99%
15	60	118	0.51	0.1341	0.0017	7.5299	0.1205	0.4057	0.0050	2154	22	2177	14	2195	23	99%
16	152	284	0.54	0.1609	0.0019	10.4349	0.1629	0.4677	0.0056	2465	14	2474	15	2473	24	99%
17	123	323	0.38	0.1591	0.0021	10.0361	0.1449	0.4547	0.0037	2446	22	2438	13	2416	17	99%
18	58	107	0.54	0.1338	0.0018	7.5169	0.1199	0.4053	0.0045	2150	23	2175	14	2193	21	99%
19	121	265	0.46	0.1348	0.0016	7.3972	0.1068	0.3952	0.0038	2161	20	2161	13	2147	18	99%
20	197	387	0.51	0.1350	0.0015	7.6130	0.1043	0.4071	0.0046	2165	18	2186	12	2202	21	99%
21	304	572	0.53	0.1349	0.0014	7.2491	0.1099	0.3871	0.0050	2165	17	2143	14	2110	23	98%
22	87	128	0.68	0.1794	0.0021	12.7429	0.1734	0.5120	0.0051	2647	19	2661	13	2665	22	99%
23	60	129	0.47	0.1371	0.0018	7.8420	0.1183	0.4122	0.0046	2190	23	2213	14	2225	21	99%
24	239	558	0.43	0.1333	0.0017	6.5930	0.0933	0.3559	0.0036	2142	22	2058	13	1963	17	95%
25	140	238	0.59	0.1478	0.0019	9.1228	0.1491	0.4440	0.0053	2321	22	2350	15	2369	24	99%
26	46	99	0.46	0.1353	0.0019	7.6436	0.1162	0.4076	0.0043	2168	24	2190	14	2204	20	99%
27	76	329	0.23	0.1936	0.0020	14.4995	0.1865	0.5396	0.0051	2773	12	2783	12	2782	22	99%
28	50	185	0.27	0.2003	0.0021	15.4689	0.1999	0.5573	0.0056	2829	17	2845	12	2855	23	99%
29	77	143	0.54	0.1378	0.0016	7.6721	0.1000	0.4016	0.0033	2200	20	2193	12	2176	15	99%
30	143	151	0.95	0.1482	0.0018	8.6812	0.1194	0.4228	0.0033	2325	20	2305	13	2273	15	98%
31	91	187	0.49	0.1375	0.0018	8.1385	0.1240	0.4275	0.0041	2198	22	2247	14	2294	19	97%
32	125	257	0.48	0.1472	0.0019	8.6649	0.1254	0.4252	0.0035	2314	22	2303	13	2284	16	99%
33	56	61	0.93	0.1354	0.0019	7.3571	0.1103	0.3938	0.0036	2169	25	2156	13	2141	17	99%
34	227	218	1.04	0.1357	0.0015	7.4235	0.1158	0.3951	0.0046	2173	19	2164	14	2147	21	99%
35	153	247	0.62	0.1345	0.0015	7.4125	0.0961	0.3980	0.0035	2158	19	2162	12	2160	16	99%
36	260	540	0.48	0.1629	0.0016	10.0944	0.1321	0.4471	0.0042	2487	17	2443	12	2382	19	97%
37	136	163	0.84	0.1491	0.0018	8.7826	0.1282	0.4258	0.0046	2336	26	2316	13	2287	21	98%
38	99	236	0.42	0.1481	0.0018	8.3866	0.1374	0.4084	0.0051	2324	20	2274	15	2207	23	97%
39	366	430	0.85	0.1114	0.0032	5.0086	0.1559	0.3205	0.0052	1833	51	1821	26	1792	25	98%
40	149	100	1.49	0.1168	0.0018	5.6354	0.0941	0.3482	0.0035	1907	32	1922	14	1926	17	99%
41	40	132	0.31	0.1372	0.0019	7.5317	0.1227	0.3958	0.0042	2192	24	2177	15	2150	20	98%
42	238	294	0.81	0.1366	0.0016	7.6320	0.1050	0.4027	0.0036	2184	20	2189	12	2182	17	99%
43	128	210	0.61	0.1371	0.0016	7.6835	0.1060	0.4040	0.0038	2191	21	2195	12	2187	17	99%
44	117	216	0.54	0.1352	0.0015	7.3404	0.0884	0.3922	0.0037	2169	20	2154	11	2133	17	99%
45	129	164	0.78	0.1666	0.0018	11.3217	0.1439	0.4903	0.0047	2524	18	2550	12	2572	20	99%
46	103	322	0.32	0.1278	0.0013	6.8406	0.0935	0.3861	0.0041	2078	19	2091	12	2104	19	99%
47	75	107	0.70	0.1341	0.0017	7.4644	0.1058	0.4022	0.0041	2154	22	2169	13	2179	19	99%
48	361	1064	0.34	0.1208	0.0014	4.8490	0.0666	0.2894	0.0028	1969	21	1793	12	1638	14	90%
49	301	485	0.62	0.1360	0.0014	6.3599	0.0739	0.3372	0.0027	2177	18	2027	10	1873	13	92%
50	138	351	0.39	0.1372	0.0013	7.6762	0.0896	0.4033	0.0033	2192	17	2194	11	2184	15	99%
51	559	524	1.07	0.1452	0.0014	7.2142	0.0724	0.3585	0.0023	2300	16	2138	9	1975	11	92%
52	286	288	0.99	0.1484	0.0015	8.5922	0.1075	0.4177	0.0039	2327	17	2296	11	2250	18	97%
53	126	302	0.42	0.1383	0.0014	7.9877	0.1081	0.4165	0.0043	2206	18	2230	12	2245	19	99%
54	111	186	0.59	0.1372	0.0014	7.6100	0.0898	0.4005	0.0033	2192	18	2186	11	2171	15	99%
55	180	291	0.62	0.1389	0.0015	7.7449	0.0911	0.4025	0.0032	2213	19	2202	11	2181	15	99%
56	141	288	0.49	0.1381	0.0016	8.0008	0.1248	0.4178	0.0049	2203	25	2231	14	2250	22	99%
59	53	106	0.50	0.1497	0.0017	8.9169	0.1554	0.4304	0.0062	2342	19	2330	16	2307	28	99%
60	102	198	0.52	0.1379	0.0013	7.9727	0.1155	0.4172	0.0048	2211	17	2228	13	2248	22	99%
61	217	516	0.42	0.1593	0.0014	9.1805	0.1147	0.4161	0.0042	2450	14	2356	12	2243	19	95%
62	124	213	0.58	0.1348	0.0013	7.6425	0.1087	0.4093	0.0046	2161	21	2190	13	2212	21	99%
63	180	488	0.37	0.1424	0.0012	7.0602	0.0768	0.3579	0.0026	2257	15	2119	10	1972	12	92%
64	128	186	0.69	0.1478	0.0014	8.8822	0.1082	0.4343	0.0041	2321	17	2326	11	2325	18	99%
65	131	205	0.64	0.1361	0.0012	7.5120	0.0947	0.3998	0.0041	2189	15	2174	11	2168	19	99%
66	137	264	0.52	0.1461	0.0011	8.8009	0.1006	0.4366	0.0042	2302	13	2318	11	2335	19	99%
67	97	161	0.61	0.1361	0.0012	7.5251	0.0908	0.4010	0.003							

Table 1 (continued)

Spot no.	Contents (ppm)		Th/U	Isotopic ratios						Age(Ma)						Concordance
	Th	U		$^{207}\text{Pb}/^{206}\text{Pb}$	1σ	$^{207}\text{Pb}/^{235}\text{U}$	1σ	$^{206}\text{Pb}/^{238}\text{U}$	1σ	$^{207}\text{Pb}/^{206}\text{Pb}$	1σ	$^{207}\text{Pb}/^{235}\text{U}$	1σ	$^{206}\text{Pb}/^{238}\text{U}$	1σ	
74	183	169	1.09	0.1372	0.0014	7.3975	0.1806	0.3893	0.0084	2192	17	2161	22	2120	39	98%
75	96	144	0.66	0.1357	0.0013	7.4533	0.0995	0.3978	0.0040	2173	18	2167	12	2159	19	99%
77	200	196	1.02	0.1368	0.0013	7.8613	0.0995	0.4155	0.0040	2187	16	2215	11	2240	18	98%
78	247	228	1.08	0.1361	0.0013	7.6184	0.0952	0.4049	0.0039	2177	17	2187	11	2191	18	99%
79	90	100	0.89	0.1480	0.0016	8.9339	0.1237	0.4360	0.0041	2324	19	2331	13	2332	18	99%
80	183	374	0.49	0.1465	0.0013	8.6571	0.0899	0.4269	0.0030	2306	11	2303	10	2292	14	99%
81	403	633	0.64	0.1900	0.0020	12.0283	0.1383	0.4565	0.0035	2742	18	2607	11	2424	15	92%
82	91	132	0.69	0.1873	0.0020	13.9603	0.1927	0.5377	0.0056	2718	17	2747	13	2774	24	99%
83	94	233	0.40	0.1346	0.0014	7.6532	0.1123	0.4094	0.0045	2161	17	2191	13	2212	21	99%
84	41	344	0.12	0.1352	0.0013	7.5679	0.0945	0.4028	0.0037	2169	16	2181	11	2182	17	99%
85	123	190	0.65	0.1337	0.0014	7.5934	0.1017	0.4087	0.0040	2148	19	2184	12	2209	19	98%
86	151	225	0.67	0.1332	0.0015	7.6495	0.1077	0.4135	0.0046	2140	19	2191	13	2231	21	98%
87	137	257	0.53	0.1339	0.0016	7.4468	0.1011	0.4003	0.0040	2150	21	2167	12	2171	19	99%
88	73	173	0.42	0.1423	0.0019	8.5967	0.1423	0.4344	0.0055	2255	24	2296	15	2326	25	98%
17XS-10																
1	43	97	0.4	0.1799	0.0024	13.0533	0.1937	0.5217	0.0056	2654	23	2684	14	2707	24	99%
2	224	215	1.0	0.1446	0.0018	8.6559	0.1234	0.4311	0.0052	2283	22	2302	13	2311	23	99%
3	123	180	0.7	0.1454	0.0017	8.7755	0.1247	0.4339	0.0046	2292	20	2315	13	2323	21	99%
4	80	151	0.5	0.1353	0.0016	7.6098	0.1271	0.4042	0.0053	2168	21	2186	15	2188	24	99%
5	102	168	0.6	0.1360	0.0016	7.7947	0.1072	0.4126	0.0045	2177	16	2208	12	2227	21	99%
8	119	189	0.6	0.1392	0.0019	7.8657	0.1213	0.4065	0.0041	2218	24	2216	14	2199	19	99%
9	58	137	0.4	0.1366	0.0019	7.9431	0.1370	0.4193	0.0053	2185	24	2225	16	2257	24	98%
10	163	262	0.6	0.1364	0.0016	7.5140	0.1007	0.3971	0.0037	2181	25	2175	12	2155	17	99%
11	381	336	1.1	0.1477	0.0016	8.2964	0.1046	0.4049	0.0033	2320	20	2264	12	2191	15	96%
12	179	171	1.0	0.1455	0.0017	8.8381	0.1255	0.4380	0.0044	2294	20	2321	13	2342	20	99%
13	61	80	0.8	0.1476	0.0020	9.0824	0.1492	0.4438	0.0049	2320	24	2346	15	2368	22	99%
14	468	611	0.8	0.1313	0.0015	5.7635	0.0993	0.3159	0.0041	2117	19	1941	15	1770	20	90%
15	196	138	1.4	0.1467	0.0019	8.7517	0.1277	0.4307	0.0040	2309	22	2312	13	2309	18	99%
16	174	192	0.9	0.1450	0.0019	8.6129	0.1288	0.4289	0.0041	2288	23	2298	14	2301	18	99%
17	231	290	0.8	0.1441	0.0018	8.5715	0.1322	0.4293	0.0045	2277	22	2294	14	2303	20	99%
18	224	197	1.1	0.1443	0.0017	8.7010	0.1355	0.4353	0.0050	2279	21	2307	14	2330	22	99%
19	253	369	0.7	0.1436	0.0016	8.0301	0.1178	0.4030	0.0044	2272	23	2234	13	2183	20	97%
20	68	141	0.5	0.1345	0.0016	7.7102	0.1097	0.4138	0.0045	2158	26	2198	13	2232	20	98%
21	140	234	0.6	0.1348	0.0015	7.7165	0.1087	0.4126	0.0044	2161	19	2199	13	2227	20	98%
22	173	217	0.8	0.1441	0.0016	8.2023	0.1173	0.4098	0.0042	2277	19	2254	13	2214	19	98%
23	161	355	0.5	0.1472	0.0018	9.0717	0.1379	0.4445	0.0057	2314	22	2345	14	2371	25	98%
24	213	352	0.6	0.1320	0.0017	6.5549	0.1238	0.3562	0.0051	2124	23	2053	17	1964	24	95%
25	135	247	0.5	0.1369	0.0015	7.8369	0.1097	0.4121	0.0044	2189	20	2212	13	2225	20	99%
26	44	82	0.5	0.1815	0.0020	13.4096	0.2140	0.5329	0.0074	2666	19	2709	15	2754	31	98%
27	37	316	0.1	0.1809	0.0017	13.4304	0.1440	0.5351	0.0042	2661	15	2710	10	2763	18	98%
28	225	396	0.6	0.1357	0.0013	7.0164	0.0907	0.3725	0.0037	2173	17	2114	12	2041	18	96%
29	193	259	0.7	0.1486	0.0014	9.0366	0.1147	0.4385	0.0042	2329	17	2342	12	2344	19	99%
30	108	100	1.1	0.1448	0.0016	8.4546	0.1079	0.4219	0.0039	2285	19	2281	12	2269	18	99%
32	172	210	0.8	0.1362	0.0014	7.7265	0.1112	0.4101	0.0048	2179	19	2200	13	2215	22	99%
33	135	174	0.8	0.1472	0.0015	8.8554	0.1168	0.4348	0.0045	2315	17	2323	12	2327	20	99%
34	191	204	0.9	0.1465	0.0014	8.8377	0.1183	0.4362	0.0049	2305	10	2321	12	2334	22	99%
35	346	364	1.0	0.1639	0.0014	10.3550	0.1241	0.4569	0.0046	2498	13	2467	11	2426	21	98%
36	117	135	0.9	0.1380	0.0013	7.6059	0.0981	0.3991	0.0043	2202	17	2186	12	2165	20	99%
37	50	99	0.5	0.1355	0.0015	7.6625	0.1031	0.4100	0.0046	2172	20	2192	12	2215	21	98%
38	350	695	0.5	0.1312	0.0009	6.1449	0.0603	0.3388	0.0026	2114	13	1997	9	1881	13	94%
39	110	240	0.5	0.1487	0.0012	8.9342	0.1069	0.4347	0.0042	2331	14	2331	11	2327	19	99%
40	93	98	0.9	0.1490	0.0015	8.0543	0.0959	0.3917	0.0033	2344	18	2237	11	2131	15	95%
41	155	255	0.6	0.1405	0.0019	8.3171	0.1213	0.4250	0.0041	2233	24	2266	13	2283	19	99%
42	170	258	0.7	0.1416	0.0017	8.1742	0.1110	0.4136	0.0038	2247	21	2250	12	2232	17	99%
43	95	147	0.6	0.1442	0.0018	8.7447	0.1150	0.4349	0.0042	2280	21	2312	12	2328	19	99%
44	163	422	0.4	0.1449	0.0016	8.8563	0.1162	0.4371	0.0048	2287	-14	2323	12	2338	22	99%
46	198	244	0.8	0.1450	0.0018	8.4835	0.1137	0.4173	0.0049	2288	-12	2284	12	2248	22	98%
47	200	219	0.9	0.1472	0.0019	8.9804	0.1233	0.4351	0.0056	2313	23	2336	13	2329	25	99%
48	79	123	0.6	0.1357	0.0020	7.7044	0.1241	0.4044	0.0060	2173	26	2197	15	2189	28	99%
49	222	217	1.0	0.1499	0.0022	8.9933	0.1349	0.4272	0.0061	2346	24	2337	14	2293	27	98%
50	274	259	1.1	0.1479	0.0020	9.2128	0.1336	0.4439	0.0060	2321	23	2359	13	2368	27	99%
51	151	232	0.6	0.1487	0.0019	9.4112	0.1339	0.4517	0.0061	2331	22	2379	13	2403	27	99%
52	125	207	0.6	0.1372	0.0017	7.8301	0.1042	0.4079	0.0049	2192	21	2212	12	2205	22	99%
53	87	148	0.6	0.1385	0.0016	7.9907	0.1017	0.4130	0.0046	2209	20	2230	12	2228	21	99%
54	92	253	0.4	0.1494	0.0017	9.3118	0.1422	0.4458	0.0056	2339	19	2369	14	2376	25	99%
55	72	89	0.8	0.1682	0.0022	11.3197	0.1704	0.4834	0.0059	2540	22	2550	14	2542	26	99%
56	308	319	1.0	0.1482	0.0017	8.4884	0.1253	0.4106	0.0051	23						

Table 1 (continued)

Spot no.	Contents (ppm)		Th/U	Isotopic ratios						Age(Ma)						Concordance
	Th	U		$^{207}\text{Pb}/^{206}\text{Pb}$	1σ	$^{207}\text{Pb}/^{235}\text{U}$	1σ	$^{206}\text{Pb}/^{238}\text{U}$	1σ	$^{207}\text{Pb}/^{206}\text{Pb}$	1σ	$^{207}\text{Pb}/^{235}\text{U}$	1σ	$^{206}\text{Pb}/^{238}\text{U}$	1σ	
63	84	205	0.4	0.1471	0.0016	8.8219	0.1144	0.4323	0.0038	2322	18	2320	12	2316	17	99%
64	189	324	0.6	0.1465	0.0017	8.7041	0.1290	0.4283	0.0046	2305	20	2308	14	2298	21	99%
65	62	129	0.5	0.1831	0.0022	13.3608	0.1961	0.5263	0.0054	2681	20	2705	14	2726	23	99%
66	126	222	0.6	0.1335	0.0016	7.2279	0.1062	0.3902	0.0038	2144	20	2140	13	2124	18	99%
67	365	617	0.6	0.1289	0.0013	5.9717	0.1105	0.3345	0.0057	2084	18	1972	16	1860	27	94%
68	407	359	1.1	0.1453	0.0014	8.4939	0.1242	0.4212	0.0049	2291	17	2285	13	2266	22	99%
69	173	294	0.6	0.1453	0.0015	8.7842	0.1223	0.4357	0.0047	2291	18	2316	13	2331	21	99%
70	113	253	0.4	0.1432	0.0016	8.6002	0.1862	0.4320	0.0080	2266	20	2297	20	2315	36	99%
71	192	343	0.6	0.1434	0.0016	8.0466	0.0960	0.4044	0.0027	2269	19	2236	11	2189	13	97%
72	50	218	0.2	0.1321	0.0017	7.5545	0.1300	0.4118	0.0051	2126	24	2179	16	2223	23	98%
73	94	342	0.3	0.1447	0.0016	8.8981	0.1202	0.4429	0.0045	2285	20	2328	12	2364	20	98%
74	26	301	0.1	0.1437	0.0015	8.6329	0.1183	0.4327	0.0045	2272	19	2300	13	2318	20	99%
75	80	119	0.7	0.2063	0.0022	16.5215	0.2076	0.5766	0.0052	2876	17	2907	12	2935	21	99%
77	197	211	0.9	0.1406	0.0015	7.9867	0.1131	0.4087	0.0045	2235	19	2230	13	2209	20	99%
78	163	322	0.5	0.1549	0.0017	9.6445	0.1391	0.4487	0.0056	2800	18	2401	13	2389	25	99%
79	76	140	0.5	0.1301	0.0016	7.4684	0.1244	0.4127	0.0053	2100	22	2169	15	2227	24	97%
17XS-19																
1	103	218	0.47	0.1301	0.0016	7.1694	0.1092	0.3967	0.0047	2099	22	2133	14	2154	22	99%
2	228	477	0.48	0.1297	0.0014	7.1887	0.0927	0.3987	0.0038	2094	18	2135	12	2163	18	98%
3	199	316	0.63	0.1306	0.0014	7.1789	0.0861	0.3957	0.0033	2106	19	2134	11	2149	15	99%
4	59	162	0.36	0.1307	0.0018	7.1358	0.0977	0.3941	0.0035	2107	24	2129	12	2142	16	99%
5	362	263	1.38	0.1142	0.0013	5.4829	0.0780	0.3462	0.0038	1866	20	1898	12	1916	18	99%
6	36	398	0.09	0.1231	0.0013	6.3491	0.0853	0.3718	0.0037	2067	19	2025	12	2038	17	99%
7	223	240	0.93	0.1421	0.0017	8.1760	0.1090	0.4151	0.0035	2254	20	2251	12	2238	16	99%
9	34	122	0.28	0.1302	0.0016	7.3341	0.1168	0.4059	0.0046	2102	22	2153	14	2196	21	98%
10	95	116	0.82	0.1262	0.0018	6.7898	0.1285	0.3871	0.0046	2056	26	2084	17	2109	21	98%
11	281	338	0.83	0.1726	0.0018	12.0822	0.1705	0.5035	0.0051	2583	17	2611	13	2629	22	99%
12	198	455	0.43	0.1274	0.0013	6.4653	0.0865	0.3649	0.0034	2063	18	2041	12	2005	16	98%
13	79	172	0.46	0.1346	0.0016	8.2181	0.1010	0.4397	0.0033	2158	25	2255	11	2349	15	95%
14	192	178	1.08	0.1396	0.0017	7.7831	0.1035	0.4015	0.0038	2222	16	2206	12	2176	17	98%
15	150	325	0.46	0.1291	0.0016	7.0580	0.1062	0.3928	0.0042	2087	22	2119	13	2136	20	99%
16	206	210	0.98	0.1373	0.0019	7.9558	0.1220	0.4162	0.0042	2194	24	2226	14	2243	19	99%
17	163	284	0.58	0.1275	0.0017	6.8955	0.1009	0.3887	0.0038	2065	24	2098	13	2117	18	99%
18	111	138	0.81	0.1408	0.0018	8.3419	0.1238	0.4260	0.0042	2237	23	2269	14	2288	19	99%
19	97	122	0.79	0.1381	0.0021	8.3794	0.1441	0.4367	0.0045	2203	28	2273	16	2336	20	97%
20	346	351	0.99	0.1374	0.0015	6.6668	0.1030	0.3489	0.0041	2195	19	2068	14	1929	20	93%
21	186	263	0.71	0.1327	0.0015	6.9668	0.0837	0.3784	0.0031	2200	19	2107	11	2069	15	98%
22	188	248	0.76	0.1311	0.0015	7.2189	0.1114	0.3968	0.0047	2113	20	2139	14	2154	22	99%
23	104	247	0.42	0.1312	0.0015	7.5531	0.1128	0.4149	0.0048	2115	53	2179	13	2237	22	97%
24	301	816	0.37	0.1248	0.0014	5.6142	0.0808	0.3242	0.0033	2026	25	1918	12	1810	16	94%
25	68	106	0.65	0.1362	0.0017	7.6522	0.1325	0.4057	0.0053	2179	27	2191	16	2195	24	99%
26	104	200	0.52	0.1365	0.0014	7.5530	0.1020	0.3999	0.0040	2184	19	2179	12	2169	19	99%
27	152	189	0.81	0.1512	0.0018	8.8911	0.1218	0.4248	0.0032	2361	20	2327	13	2282	15	98%
28	151	182	0.83	0.1285	0.0013	6.8382	0.0921	0.3850	0.0037	2077	19	2091	12	2100	17	99%
29	139	300	0.46	0.1481	0.0012	8.7241	0.0844	0.4260	0.0030	2324	14	2310	9	2288	14	99%
30	91	161	0.56	0.1503	0.0013	8.9498	0.0908	0.4310	0.0032	2350	10	2333	9	2310	14	99%
31	234	260	0.90	0.1490	0.0013	7.9164	0.0973	0.3846	0.0039	2344	15	2222	11	2098	18	94%
32	114	313	0.36	0.1362	0.0012	7.4457	0.0805	0.3957	0.0033	2180	15	2166	10	2149	15	99%
33	63	149	0.42	0.1302	0.0013	6.9259	0.0917	0.3850	0.0038	2102	17	2102	12	2099	18	99%
34	461	545	0.85	0.1452	0.0012	7.1747	0.0757	0.3575	0.0027	2290	15	2133	10	1970	13	92%
35	129	324	0.40	0.1312	0.0010	7.1444	0.0939	0.3941	0.0044	2115	13	2130	12	2142	21	99%
36	93	245	0.38	0.1377	0.0011	7.5773	0.0764	0.3985	0.0031	2198	14	2182	9	2162	14	99%
37	136	168	0.81	0.1376	0.0012	7.4063	0.0858	0.3898	0.0035	2198	15	2162	10	2122	16	98%
38	65	72	0.91	0.1493	0.0015	8.9950	0.1144	0.4372	0.0044	2339	17	2337	12	2338	20	99%
39	71	229	0.31	0.1487	0.0011	9.1023	0.1133	0.4435	0.0048	2331	12	2348	11	2366	22	99%
40	72	210	0.34	0.1453	0.0013	8.6932	0.1509	0.4347	0.0073	2291	16	2306	16	2327	33	99%
41	236	436	0.54	0.1341	0.0011	6.7443	0.0660	0.3644	0.0026	2154	14	2078	9	2003	12	96%
42	575	499	1.15	0.1444	0.0011	7.4398	0.1138	0.3730	0.0051	2281	13	2166	14	2043	24	94%
43	213	293	0.73	0.1357	0.0011	7.5027	0.0929	0.4003	0.0037	2173	14	2173	11	2170	17	99%
44	76	207	0.37	0.1345	0.0012	7.5229	0.0950	0.4048	0.0038	2158	17	2176	11	2191	17	99%
45	52	483	0.11	0.1272	0.0012	6.7644	0.0925	0.3851	0.0041	2061	16	2081	12	2100	19	99%
46	109	282	0.38	0.1359	0.0014	7.6049	0.1048	0.4048	0.0036	2176	19	2185	12	2191	16	99%
47	50	318	0.16	0.1294	0.0015	6.9398	0.1046	0.3878	0.0038	2090	20	2104	13	2113	18	99%
48	66	191	0.35	0.1825	0.0023	13.1889	0.2190	0.5224	0.0054	2676	22	2693	16	2710	23	99%
49	86	113	0.76	0.1358	0.0019	7.7085	0.1339	0.4102	0.0040	2174	24	2198	16	2216	19	99%
50	249	949	0.26	0.1235	0.0014	5.6739	0.0879	0.3317	0.0034	2007	20	1927	13	1847	17	95%
51	57</															

Table 1 (continued)

Spot no.	Contents (ppm)		Th/U	Isotopic ratios						Age(Ma)						Concordance
	Th	U		$^{207}\text{Pb}/^{206}\text{Pb}$	1σ	$^{207}\text{Pb}/^{235}\text{U}$	1σ	$^{206}\text{Pb}/^{238}\text{U}$	1σ	$^{207}\text{Pb}/^{206}\text{Pb}$	1σ	$^{207}\text{Pb}/^{235}\text{U}$	1σ	$^{206}\text{Pb}/^{238}\text{U}$	1σ	
61	103	122	0.84	0.1356	0.0017	7.4207	0.0999	0.3943	0.0036	2172	22	2163	12	2143	17	99%
63	325	530	0.61	0.1447	0.0018	8.4936	0.1321	0.4219	0.0048	2284	22	2285	14	2269	22	99%
64	194	318	0.61	0.1476	0.0021	8.8001	0.1311	0.4286	0.0042	2318	24	2318	14	2299	19	99%
65	139	320	0.43	0.1388	0.0025	8.2966	0.1684	0.4306	0.0051	2213	31	2264	18	2308	23	98%
66	230	465	0.49	0.1290	0.0021	6.3206	0.1159	0.3531	0.0037	2084	33	2021	16	1949	18	96%
67	184	280	0.66	0.1410	0.0020	8.3413	0.1373	0.4263	0.0043	2239	25	2269	15	2289	20	99%
68	124	215	0.58	0.1326	0.0018	7.4627	0.1145	0.4059	0.0040	2132	29	2169	14	2196	18	98%
69	264	316	0.84	0.1430	0.0017	8.5640	0.1152	0.4316	0.0040	2265	21	2293	12	2313	18	99%
70	178	406	0.44	0.1220	0.0015	5.7602	0.0764	0.3403	0.0032	1987	21	1940	12	1888	15	97%
71	285	553	0.52	0.1318	0.0015	6.0268	0.0806	0.3291	0.0030	2124	21	1980	12	1834	15	92%
72	168	96	1.74	0.1468	0.0021	8.1207	0.1922	0.3975	0.0078	2309	30	2245	21	2158	36	96%
73	155	366	0.42	0.1311	0.0016	6.6292	0.1065	0.3637	0.0044	2122	55	2063	14	2000	21	96%
74	107	236	0.45	0.1452	0.0017	8.6861	0.1224	0.4309	0.0045	2290	20	2306	13	2310	20	99%
76	69	116	0.60	0.1209	0.0016	6.1889	0.1261	0.3686	0.0062	1970	24	2003	18	2023	29	99%
77	85	100	0.85	0.1471	0.0017	8.9828	0.1190	0.4399	0.0040	2313	19	2336	12	2350	18	99%
78	47	71	0.67	0.1393	0.0019	8.5003	0.1442	0.4394	0.0051	2220	23	2286	15	2348	23	97%
79	97	313	0.31	0.1331	0.0014	7.4203	0.1146	0.4003	0.0042	2140	19	2163	14	2170	19	99%
81	155	261	0.59	0.1365	0.0017	7.7597	0.1160	0.4103	0.0043	2184	22	2204	14	2216	20	99%
82	269	818	0.33	0.1226	0.0014	5.3919	0.0883	0.3173	0.0040	1994	20	1884	14	1777	20	94%
84	152	163	0.93	0.1450	0.0017	8.7092	0.1220	0.4346	0.0047	2289	20	2308	13	2327	21	99%
85	215	338	0.64	0.1459	0.0015	8.2380	0.1051	0.4084	0.0038	2298	18	2258	12	2208	17	97%
86	90	156	0.58	0.1338	0.0016	7.4623	0.0999	0.4047	0.0042	2150	21	2168	12	2190	19	98%
87	130	152	0.85	0.1321	0.0017	7.3686	0.1151	0.4044	0.0047	2126	24	2157	14	2189	22	98%
88	36	142	0.25	0.1246	0.0017	6.4859	0.0953	0.3779	0.0038	2033	25	2044	13	2066	18	98%
18XS-2																
1	200	468	0.43	0.1418	0.0022	8.1503	0.1719	0.4145	0.0068	2250	27	2248	19	2235	31	99%
2	119	222	0.54	0.1347	0.0018	7.5998	0.1146	0.4064	0.0044	2161	23	2185	14	2199	20	99%
4	166	257	0.65	0.1959	0.0023	14.4949	0.2516	0.5321	0.0076	2792	19	2783	17	2750	32	98%
5	154	146	1.05	0.1639	0.0020	11.2149	0.1804	0.4933	0.0067	2498	21	2541	15	2585	29	98%
6	106	163	0.65	0.1377	0.0018	7.9653	0.1260	0.4169	0.0051	2198	22	2227	14	2246	23	99%
7	81	180	0.45	0.1357	0.0019	7.6143	0.1279	0.4046	0.0053	2173	24	2187	15	2190	24	99%
8	185	346	0.53	0.1447	0.0021	8.4754	0.1379	0.4205	0.0043	2285	24	2283	15	2263	20	99%
9	102	154	0.66	0.1370	0.0021	7.9271	0.1441	0.4162	0.0051	2191	27	2223	16	2243	23	99%
10	110	162	0.68	0.1830	0.0026	13.1962	0.2146	0.5186	0.0058	2681	23	2694	15	2693	25	99%
11	137	166	0.82	0.1350	0.0019	7.6748	0.1368	0.4088	0.0054	2165	24	2194	16	2209	25	99%
12	167	200	0.83	0.1461	0.0018	8.5819	0.1153	0.4231	0.0037	2302	21	2295	12	2275	17	99%
13	90	167	0.54	0.1351	0.0018	7.6213	0.1118	0.4074	0.0046	2165	23	2187	13	2203	21	99%
14	122	172	0.71	0.1325	0.0024	7.6285	0.1346	0.4086	0.0059	2131	31	2188	16	2208	27	99%
15	124	192	0.65	0.1345	0.0017	7.7294	0.1205	0.4138	0.0046	2158	23	2200	14	2232	21	98%
16	84	84	1.00	0.1448	0.0022	8.3888	0.1377	0.4182	0.0042	2285	32	2274	15	2252	19	99%
17	133	191	0.70	0.1331	0.0020	7.3392	0.1166	0.3977	0.0035	2139	21	2154	14	2158	16	99%
18	244	306	0.80	0.1470	0.0020	8.5939	0.1456	0.4206	0.0046	2322	28	2296	15	2263	21	98%
19	40	56	0.71	0.1477	0.0023	8.7589	0.1392	0.4289	0.0041	2320	26	2313	15	2301	19	99%
20	121	163	0.74	0.1458	0.0018	8.8911	0.1412	0.4396	0.0050	2298	21	2327	15	2349	23	99%
21	97	111	0.88	0.1340	0.0019	7.4832	0.1191	0.4033	0.0042	2150	25	2171	14	2184	19	99%
22	126	264	0.48	0.1613	0.0020	10.3167	0.1443	0.4609	0.0041	2469	20	2464	13	2444	18	99%
23	144	187	0.77	0.1452	0.0023	8.8668	0.1605	0.4375	0.0061	2300	27	2324	17	2339	27	99%
24	42	86	0.48	0.1585	0.0030	10.1242	0.2567	0.4566	0.0059	2439	33	2446	23	2424	26	99%
25	116	264	0.44	0.1344	0.0021	7.5118	0.1757	0.4035	0.0076	2167	27	2174	21	2185	35	99%
26	174	194	0.90	0.1458	0.0020	8.7916	0.1413	0.4349	0.0047	2298	24	2317	15	2328	21	99%
27	200	464	0.43	0.1772	0.0021	12.3242	0.1748	0.5012	0.0046	2627	20	2629	13	2619	20	99%
28	178	316	0.56	0.1345	0.0016	7.5230	0.1311	0.4028	0.0053	2158	21	2176	16	2182	24	99%
29	254	358	0.71	0.1450	0.0017	8.5652	0.1242	0.4258	0.0044	2288	21	2293	13	2287	20	99%
30	66	121	0.54	0.1812	0.0023	13.0908	0.2002	0.5219	0.0060	2665	21	2686	15	2707	25	99%
31	69	172	0.40	0.1366	0.0018	7.7900	0.1313	0.4108	0.0047	2185	23	2207	15	2219	22	99%
34	126	193	0.65	0.1353	0.0018	7.4362	0.1123	0.3962	0.0035	2168	24	2165	14	2151	16	99%
35	188	246	0.76	0.1646	0.0020	10.9770	0.1615	0.4808	0.0048	2503	20	2521	14	2531	21	99%
36	151	270	0.56	0.1462	0.0018	8.9212	0.1437	0.4403	0.0056	2302	21	2330	15	2352	25	99%
38	201	273	0.74	0.1340	0.0017	7.5533	0.1245	0.4035	0.0049	2152	23	2179	15	2197	22	99%
39	115	123	0.93	0.1468	0.0023	8.8010	0.1639	0.4319	0.0054	2309	26	2318	17	2314	24	99%
40	203	236	0.86	0.1614	0.0026	10.3107	0.1921	0.4599	0.0054	2472	27	2463	17	2439	24	99%
41	34	230	0.15	0.1424	0.0024	8.4532	0.1582	0.4288	0.0058	2257	28	2281	17	2300	26	99%
42	162	407	0.40	0.1443	0.0021	8.5727	0.1526	0.4276	0.0052	2280	25	2294	16	2295	24	99%
43	231	455	0.51	0.1350	0.0018	6.8302	0.0933	0.3647	0.0025	2165	24	2090	12	2004	12	95%
44	167	385	0.43	0.1342	0.0017	7.5603	0.1174	0.4063	0.0046	2154	22	2180	14	2198	21	99%
45	60	104	0.58	0.1357	0.0020	7.6353	0.1318	0.4070	0.0053	2173	26	2189	16	2201	24	

Table 1 (continued)

Spot no.	Contents (ppm)		Th/U	Isotopic ratios						Age(Ma)						Concordance
	Th	U		$^{207}\text{Pb}/^{206}\text{Pb}$	1σ	$^{207}\text{Pb}/^{235}\text{U}$	1σ	$^{206}\text{Pb}/^{238}\text{U}$	1σ	$^{207}\text{Pb}/^{206}\text{Pb}$	1σ	$^{207}\text{Pb}/^{235}\text{U}$	1σ	$^{206}\text{Pb}/^{238}\text{U}$	1σ	
53	191	281	0.68	0.1470	0.0017	8.6418	0.1329	0.4240	0.0045	2311	20	2301	14	2279	20	99%
54	58	123	0.47	0.1352	0.0018	7.6254	0.1189	0.4071	0.0041	2169	23	2188	14	2202	19	99%
55	233	282	0.83	0.1347	0.0018	6.9146	0.1165	0.3704	0.0042	2161	24	2101	15	2031	20	96%
56	199	373	0.53	0.1318	0.0019	6.9666	0.1121	0.3818	0.0037	2122	24	2107	14	2085	18	98%
57	79	183	0.43	0.1467	0.0022	8.9016	0.1515	0.4386	0.0047	2309	31	2328	16	2344	21	99%
58	133	197	0.68	0.1355	0.0019	7.3840	0.1170	0.3930	0.0035	2172	25	2159	14	2137	16	98%
59	142	225	0.63	0.1342	0.0018	7.0578	0.0991	0.3796	0.0028	2153	22	2119	13	2074	13	97%
60	72	125	0.57	0.1358	0.0018	7.6709	0.1200	0.4084	0.0047	2176	24	2193	14	2208	22	99%
61	391	463	0.84	0.1308	0.0015	5.9219	0.0767	0.3267	0.0027	2109	21	1964	11	1822	13	92%
62	229	237	0.97	0.1455	0.0017	8.7715	0.1219	0.4350	0.0045	2294	20	2315	13	2328	20	99%
63	122	126	0.97	0.1460	0.0019	8.8157	0.1455	0.4357	0.0054	2300	23	2319	15	2331	24	99%
64	159	343	0.46	0.1342	0.0016	6.5166	0.0957	0.3500	0.0036	2153	22	2048	13	1935	17	94%
65	124	147	0.84	0.1353	0.0022	7.6975	0.1518	0.4114	0.0049	2169	28	2196	18	2221	22	98%
66	78	149	0.52	0.1360	0.0019	7.7445	0.1220	0.4119	0.0039	2177	29	2202	14	2224	18	99%
67	123	182	0.68	0.1360	0.0018	7.7133	0.1320	0.4098	0.0050	2177	23	2198	15	2214	23	99%
68	208	184	1.14	0.1485	0.0019	8.7597	0.1348	0.4260	0.0042	2328	22	2313	14	2288	19	98%
69	163	229	0.71	0.1379	0.0017	7.6192	0.1051	0.3990	0.0036	2211	21	2187	12	2165	16	98%
70	134	161	0.83	0.1395	0.0019	8.0513	0.1301	0.4170	0.0049	2221	23	2237	15	2247	22	99%
71	119	208	0.57	0.1518	0.0020	9.3245	0.1403	0.4433	0.0044	2366	24	2370	14	2365	20	99%
72	313	301	1.04	0.1484	0.0021	8.8083	0.1698	0.4279	0.0063	2327	25	2318	18	2296	28	99%
73	54	187	0.29	0.1857	0.0028	13.0041	0.2002	0.5046	0.0039	2706	25	2680	15	2633	17	98%
74	194	267	0.73	0.1509	0.0021	9.1170	0.1434	0.4353	0.0043	2367	23	2350	14	2329	19	99%
75	81	152	0.53	0.1389	0.0019	7.9937	0.1351	0.4169	0.0057	2213	24	2230	15	2247	26	99%
76	211	250	0.85	0.1473	0.0018	8.6818	0.1141	0.4250	0.0033	2317	21	2305	12	2283	15	99%
77	153	198	0.78	0.1364	0.0016	7.7639	0.1285	0.4101	0.0051	2183	21	2204	15	2215	23	99%
78	122	201	0.61	0.1485	0.0017	9.1115	0.1355	0.4424	0.0047	2329	21	2349	14	2361	21	99%
79	153	218	0.70	0.1474	0.0017	8.8116	0.1236	0.4310	0.0042	2316	19	2319	13	2310	19	99%
80	95	218	0.44	0.1348	0.0016	7.3506	0.1029	0.3935	0.0036	2161	22	2155	13	2139	17	99%

near-concordant and give U-Pb ages with wide apparent $^{206}\text{Pb}/^{207}\text{Pb}$ age range of 2.08–2.88 Ga, forming a remarkable age peak at ~2.30 Ga (Fig. 5). The youngest concordant zircon in this sample yields a $^{207}\text{Pb}/^{206}\text{Pb}$ age of 2100 ± 22 Ma.

4.1.3. 17XS-19 (quartzite sample)

The majority of zircons from the quartzite sample 17XS-19 are subhedral, subrounded to subangular, range in size from 50 μm to 250 μm. Most zircons have clearly oscillatory growth zonings (Fig. 5). 80 analyses give concordant or near-concordant $^{207}\text{Pb}/^{206}\text{Pb}$ ages cluster at 1.87–2.68 Ga, with three major age peaks at ~2.11 Ga, 2.18 Ga, and 2.29 Ga (Fig. 5). These zircons have Th contents of 34–575 ppm, U contents of 71–949 ppm, and Th/U ratios of 0.09–1.74 (0.61 on average), indicating a magmatic origin (Vavra et al., 1999; Hoskin and Black, 2000). The youngest concordant zircon has $^{207}\text{Pb}/^{206}\text{Pb}$ age of 1866 ± 20 Ma.

4.1.4. 18XS-2 (feldspar quartzite sample)

Zircons from sample 18XS-2 are mostly subrounded to subangular with length/width ratios of 1:1–3:1. According to the CL images, most zircons exhibit oscillatory zonings, with minor showing homogenous or mottled textures with or without metamorphic rim, implying secondary modification (Fig. 5). These features, together with their variable Th (35–559 ppm), U (56–468 ppm) concentrations and Th/U ratios (0.15–2.40), imply a magmatic origin of these zircons (Vavra et al., 1999; Hoskin and Black, 2000). 76 analyses are concordant on the U-Pb concordia diagram (Fig. 5), yielding $^{207}\text{Pb}/^{206}\text{Pb}$ ages between 2.79 Ga and 2.11 Ga, with two prominent age peaks at ~1.7 Ga and 2.31 Ga, and three sub peaks at ~2.49 Ga, 2.67 Ga and 2.79 Ga (Fig. 5). The youngest concordant $^{207}\text{Pb}/^{206}\text{Pb}$ age is 2109 ± 20 Ma.

4.2. In situ zircon Lu-Hf isotopes

197 zircons with concordant U-Pb ages were selected for *in-situ* Lu-Hf isotopic analyses. The results are given in Table 2.

The analyzed detrital zircons can be broadly subdivided into

Neoarchean and Paleoproterozoic age groups (Fig. 6a). For the Neoarchean zircons (22 grains), their $^{176}\text{Lu}/^{177}\text{Hf}$ and $^{176}\text{Hf}/^{177}\text{Hf}$ ratios range from 0.000264 to 0.001867, and 0.281030 to 0.281453, respectively. All zircons, except for 2 grain (−0.8 to −0.7), have positive $\epsilon_{\text{Hf}}(t)$ values from 0.1 to 8.9 (Fig. 6b), with the model age T_{DM}^1 and T_{DM}^{C} of 2.50–3.09 Ga and 2.51–3.26 Ga, suggesting their origin from a juvenile crust. For the dominant Paleoproterozoic zircon population, their $^{176}\text{Lu}/^{177}\text{Hf}$ and $^{176}\text{Hf}/^{177}\text{Hf}$ ratios range from 0.000051 to 0.003291, and 0.281166 to 0.281706, respectively. They have a wide range of $\epsilon_{\text{Hf}}(t)$ values of −7.3 to 8.9 (Fig. 6b), with the model age T_{DM}^1 and T_{DM}^{C} of 2.19–2.88 Ga and 2.25–3.29 Ga, indicative of the mixing of a Neoarchean crust with juvenile crustal additions.

4.3. Whole-rock major and trace element geochemistry

Whole-rock major and trace element data of the Fangniushan metasedimentary rocks are listed in Table 3. The quartzite samples are characterized by variable contents of SiO_2 (67.51–96.88 wt%), Al_2O_3 (1.29–16.97 wt%) and $\text{K}_2\text{O} + \text{N}_2\text{O}$ (0.50–8.40 wt%). Concentrations of CaO , $\text{Fe}_2\text{O}_3 + \text{MgO}$, and TiO_2 are low in the analyzed samples, ranging from 0.03 to 2.94 wt%, 0.86–4.11 wt%, and 0.03–0.39 wt%, respectively. On the sediment classification diagram of Herron (1988), most of the Fangniushan metasedimentary rocks share similar geochemical characteristics, as shown by their respective $\log(\text{SiO}_2/\text{Al}_2\text{O}_3)$ (0.61 to 1.88) and $\log(\text{Fe}_2\text{O}_3/\text{K}_2\text{O})$ (−0.33 to 0.33) values. These rocks are plotted mainly within the arkose and subarkose field (Fig. 7).

The total REE contents of the samples range between 16.40 and 559.69 ppm (147.03 ppm on average), similar to the upper continental crust (UCC) (148.44 ppm) and Post-Archean Australian Shale (PAAS) (184.77 ppm) (Taylor and McLennan, 1985). Except for 3 samples (17XS-11, 17XS-22 and 17XS-24), the sedimentary rocks have broadly similar chondrite-normalized REE patterns, with obvious enriched LREE ($(\text{La/Yb})_N = 5.50$ –115.43), relatively flat HREE ($(\text{Gd/Yb})_N = 0.83$ –6.57) and negative Eu anomalies ($\text{Eu/Eu}^* = 0.50$ –1.03) (Fig. 8a), similarly to those of the PAAS (Taylor and McLennan, 1985). Besides, most of samples have very flat upper continental crust (UCC)-

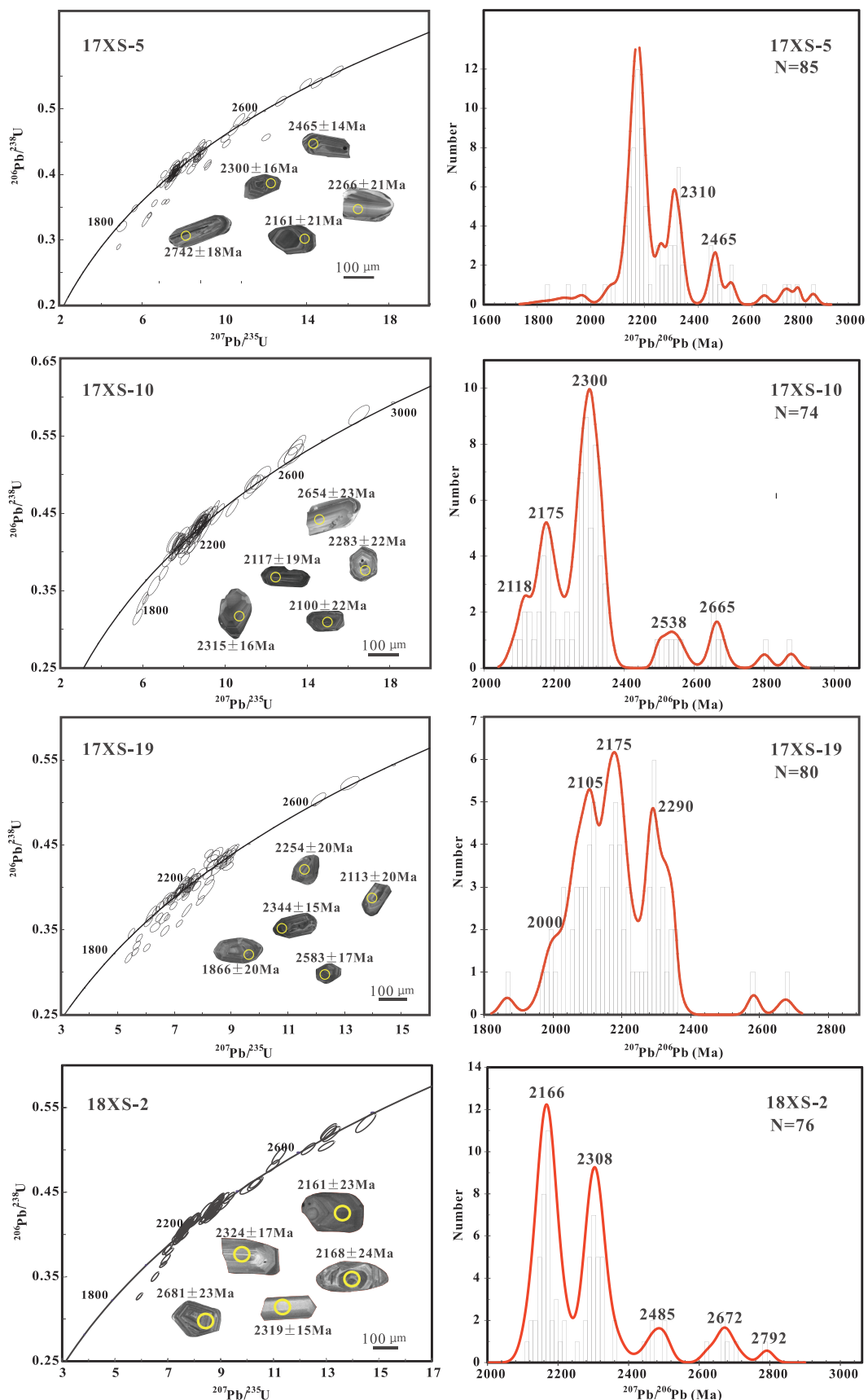


Fig. 5. Zircon U-Pb concordia diagrams and histograms of concordant zircon $^{207}\text{Pb}/^{206}\text{Pb}$ ages for three samples of Fangniushan metasedimentary rocks. Representative Cathode-luminescence (CL) images of zircons are inserted in each diagram.

Table 2

Detrital zircon Lu-Hf isotope compositions of the Fangniushan metasedimentary rocks in the Xiaoshan area.

Spot no.	Age (Ma)	$^{176}\text{Yb}/^{177}\text{Hf}$	$^{176}\text{Lu}/^{177}\text{Hf}$	$^{176}\text{Hf}/^{177}\text{Hf}$	2σ	$\epsilon_{\text{Hf}}(0)$	$\epsilon_{\text{Hf}}(t)$	T_{DM1} (Ma)	T_{DM}^{C} (Ma)	$f_{\text{Lu/Hf}}$
17XS-5-1	2177	0.040274	0.000919	0.281406	0.000012	-48.4	-1.1	2578	2844	-0.97
17XS-5-2	2266	0.031381	0.000660	0.281523	0.000015	-44.3	5.4	2402	2495	-0.98
17XS-5-3	2306	0.027865	0.000609	0.281219	0.000013	-55.0	-4.4	2809	3152	-0.98
17XS-5-4	2172	0.038769	0.000777	0.281493	0.000015	-45.3	2.1	2450	2637	-0.98
17XS-5-5	2146	0.053669	0.001110	0.281443	0.000015	-47.1	-0.7	2541	2799	-0.97
17XS-5-6	2277	0.025304	0.000564	0.281314	0.000013	-51.6	-1.6	2678	2952	-0.98
17XS-5-7	2058	0.038725	0.000787	0.281540	0.000015	-43.6	1.2	2387	2606	-0.98
17XS-5-9	2127	0.026042	0.000566	0.281525	0.000012	-44.2	2.6	2393	2574	-0.98
17XS-5-10	2131	0.044749	0.000947	0.281436	0.000016	-47.3	-1.1	2539	2808	-0.97
17XS-5-11	2121	0.047043	0.000999	0.281371	0.000015	-49.6	-3.7	2631	2967	-0.97
17XS-5-12	2276	0.051115	0.001151	0.281334	0.000015	-50.9	-1.8	2692	2964	-0.97
17XS-5-13	2455	0.055182	0.001147	0.281391	0.000016	-48.9	4.2	2614	2720	-0.97
17XS-5-14	2246	0.041224	0.000887	0.281362	0.000014	-49.9	-1.1	2636	2896	-0.97
17XS-5-15	2154	0.044754	0.000938	0.281451	0.000014	-46.8	0.0	2518	2760	-0.97
17XS-5-16	2465	0.030840	0.000708	0.281318	0.000014	-51.5	2.6	2683	2833	-0.98
17XS-5-17	2446	0.031913	0.000644	0.281453	0.000013	-46.7	7.1	2496	2530	-0.98
17XS-5-18	2150	0.034886	0.000705	0.281439	0.000016	-47.2	-0.2	2519	2768	-0.98
17XS-5-19	2161	0.029091	0.000637	0.281447	0.000014	-46.9	0.4	2504	2736	-0.98
17XS-5-20	2165	0.038044	0.000773	0.281450	0.000013	-46.8	0.4	2509	2740	-0.98
17XS-5-21	2165	0.059301	0.001257	0.281449	0.000012	-46.8	-0.3	2541	2785	-0.96
17XS-5-22	2647	0.042043	0.000900	0.281145	0.000014	-57.6	0.2	2931	3124	-0.97
17XS-5-23	2190	0.041733	0.000833	0.281541	0.000015	-43.6	4.2	2388	2520	-0.97
17XS-5-24	2142	0.069828	0.001438	0.281540	0.000013	-43.6	2.2	2428	2611	-0.96
17XS-5-25	2321	0.033565	0.000721	0.281347	0.000013	-50.5	0.3	2645	2864	-0.98
17XS-5-26	2168	0.034601	0.000701	0.281463	0.000014	-46.3	1.1	2485	2699	-0.98
17XS-5-27	2773	0.023295	0.000496	0.281068	0.000011	-60.3	1.1	3003	3165	-0.99
17XS-5-30	2325	0.047748	0.001040	0.281306	0.000017	-51.9	-1.5	2722	2986	-0.97
17XS-5-31	2198	0.030769	0.000653	0.281417	0.000012	-48.0	0.2	2545	2781	-0.98
17XS-5-32	2314	0.035427	0.000739	0.281292	0.000014	-52.4	-1.8	2720	2994	-0.98
17XS-5-33	2169	0.038592	0.000746	0.281355	0.000015	-50.2	-2.8	2635	2948	-0.98
17XS-5-34	2173	0.086833	0.001682	0.281527	0.000014	-44.1	2.0	2462	2644	-0.95
17XS-5-35	2158	0.034099	0.000672	0.281400	0.000013	-48.6	-1.4	2569	2847	-0.98
17XS-5-36	2487	0.038907	0.000880	0.281279	0.000014	-52.9	1.4	2747	2924	-0.97
17XS-5-37	2336	0.039998	0.000883	0.281277	0.000016	-52.9	-2.1	2750	3028	-0.97
17XS-5-38	2324	0.051399	0.001218	0.281346	0.000017	-50.5	-0.4	2680	2913	-0.96
17XS-5-40	1907	0.032725	0.000653	0.281494	0.000015	-45.3	-3.6	2441	2797	-0.98
17XS-5-42	2184	0.044897	0.000929	0.281506	0.000013	-44.8	2.6	2442	2614	-0.97
17XS-5-44	2169	0.037012	0.000756	0.281449	0.000015	-46.8	0.5	2508	2736	-0.98
17XS-5-45	2524	0.044316	0.000886	0.281308	0.000016	-51.8	3.3	2709	2834	-0.97
17XS-5-46	2078	0.026055	0.000543	0.281608	0.000013	-41.2	4.4	2279	2416	-0.98
17XS-5-47	2154	0.033720	0.000716	0.281576	0.000014	-42.4	4.7	2334	2455	-0.98
17XS-5-48	1969	0.056483	0.001143	0.281544	0.000016	-43.5	-1.1	2403	2684	-0.97
17XS-5-49	2177	0.034274	0.000751	0.281418	0.000013	-48.0	-0.4	2550	2801	-0.98
17XS-5-50	2192	0.028921	0.000631	0.281386	0.000015	-49.1	-1.0	2585	2852	-0.98
17XS-5-53	2206	0.046454	0.001041	0.281486	0.000016	-45.5	2.2	2476	2655	-0.97
17XS-5-54	2192	0.023037	0.000536	0.281389	0.000014	-49.0	-0.8	2575	2836	-0.98
17XS-5-55	2213	0.040178	0.000818	0.281394	0.000015	-48.8	-0.6	2588	2839	-0.98
17XS-5-56	2203	0.032097	0.000670	0.281407	0.000015	-48.4	-0.1	2560	2802	-0.98
17XS-5-59	2342	0.030357	0.000640	0.281260	0.000013	-53.5	-2.1	2757	3039	-0.98
17XS-5-60	2211	0.024770	0.000535	0.281505	0.000015	-44.9	3.8	2419	2561	-0.98
17XS-5-61	2450	0.023487	0.000530	0.281290	0.000010	-52.5	1.5	2709	2888	-0.98
17XS-5-62	2161	0.032928	0.000727	0.281493	0.000012	-45.3	1.9	2447	2640	-0.98
17XS-5-64	2321	0.065005	0.001329	0.281483	0.000013	-45.6	4.2	2499	2615	-0.96
17XS-5-65	2189	0.071052	0.001439	0.281555	0.000017	-43.1	3.7	2407	2547	-0.96
17XS-5-66	2302	0.058715	0.001472	0.281342	0.000012	-50.7	-1.4	2705	2964	-0.96
17XS-5-67	2177	0.039509	0.000775	0.281538	0.000012	-43.7	3.9	2388	2529	-0.98
17XS-5-68	2468	0.040929	0.000800	0.281393	0.000012	-48.8	5.2	2587	2669	-0.98
17XS-5-69	2261	0.075917	0.001676	0.281434	0.000014	-47.4	0.7	2590	2799	-0.95
17XS-5-70	2120	0.041654	0.000821	0.281474	0.000012	-46.0	0.2	2479	2717	-0.98
17XS-5-71	2524	0.031962	0.000674	0.281402	0.000016	-48.5	6.9	2567	2597	-0.98
17XS-5-72	2322	0.030568	0.000665	0.281361	0.000013	-50.0	1.0	2622	2826	-0.98
17XS-5-74	2192	0.076734	0.001590	0.281561	0.000013	-42.9	3.8	2408	2546	-0.95
17XS-5-75	2173	0.044359	0.000914	0.281374	0.000016	-49.5	-2.3	2621	2919	-0.97
17XS-5-77	2187	0.058274	0.001344	0.281513	0.000013	-44.6	2.3	2459	2634	-0.96
17XS-5-78	2177	0.019594	0.000416	0.281293	0.000013	-52.4	-4.4	2697	3053	-0.99
17XS-5-79	2324	0.031554	0.000762	0.281340	0.000016	-50.7	0.1	2657	2882	-0.98
17XS-5-80	2306	0.031802	0.000664	0.281340	0.000012	-50.7	-0.1	2650	2883	-0.98
17XS-5-81	2742	0.082331	0.001867	0.281265	0.000017	-53.3	4.8	2839	2901	-0.94
17XS-5-82	2718	0.042155	0.000922	0.281065	0.000012	-60.4	-1.1	3041	3261	-0.97
17XS-5-83	2161	0.064005	0.001334	0.281543	0.000011	-43.5	2.8	2417	2582	-0.96
17XS-5-84	2169	0.002702	0.000051	0.281339	0.000014	-50.8	-2.4	2611	2921	-1.00
17XS-5-85	2148	0.043637	0.000943	0.281533	0.000016	-43.9	2.8	2405	2576	-0.97
17XS-5-87	2150	0.041769	0.000796	0.281411	0.000013	-48.2	-1.3	2562	2838	-0.98
17XS-5-88	2255	0.020919	0.000458	0.281214	0.000012	-55.2	-5.4	2805	3182	-0.99

(continued on next page)

Table 2 (continued)

Spot no.	Age (Ma)	$^{176}\text{Yb}/^{177}\text{Hf}$	$^{176}\text{Lu}/^{177}\text{Hf}$	$^{176}\text{Hf}/^{177}\text{Hf}$	2σ	$\epsilon_{\text{Hf}}(0)$	$\epsilon_{\text{Hf}}(\text{t})$	T_{DM1} (Ma)	T_{DM}^{c} (Ma)	$f_{\text{Lu/Hf}}$
17XS-10-01	2654	0.014626	0.000357	0.281134	0.000017	-58.0	0.9	2906	3083	-0.99
17XS-10-03	2292	0.028183	0.000655	0.281324	0.000016	-51.3	-1.0	2671	2928	-0.98
17XS-10-04	2168	0.028934	0.000571	0.281321	0.000016	-51.4	-3.8	2670	3009	-0.98
17XS-10-05	2177	0.055019	0.001148	0.281599	0.000017	-41.5	5.5	2327	2426	-0.97
17XS-10-08	2218	0.043866	0.001014	0.281569	0.000014	-42.6	5.5	2361	2456	-0.97
17XS-10-09	2185	0.043284	0.000943	0.281405	0.000015	-48.4	-1.0	2581	2844	-0.97
17XS-10-11	2320	0.045197	0.000998	0.281289	0.000015	-52.5	-2.2	2742	3023	-0.97
17XS-10-12	2294	0.035893	0.000768	0.281383	0.000017	-49.2	0.9	2599	2805	-0.98
17XS-10-13	2320	0.021938	0.000470	0.281166	0.000015	-56.9	-5.7	2870	3248	-0.99
17XS-10-15	2309	0.086922	0.001888	0.281310	0.000018	-51.8	-3.0	2778	3071	-0.94
17XS-10-16	2288	0.025299	0.000583	0.281245	0.000014	-54.1	-3.8	2773	3103	-0.98
17XS-10-17	2277	0.058218	0.001314	0.281360	0.000017	-50.0	-1.1	2668	2922	-0.96
17XS-10-18	2279	0.048816	0.001119	0.281252	0.000015	-53.8	-4.6	2801	3145	-0.97
17XS-10-19	2272	0.055090	0.001167	0.281367	0.000014	-49.8	-0.7	2648	2895	-0.96
17XS-10-20	2158	0.049098	0.001002	0.281478	0.000014	-45.8	0.9	2485	2701	-0.97
17XS-10-21	2161	0.035764	0.000856	0.281365	0.000015	-49.8	-2.8	2629	2941	-0.97
17XS-10-22	2277	0.042692	0.000937	0.281377	0.000015	-49.4	0.1	2619	2847	-0.97
17XS-10-23	2314	0.052811	0.001194	0.281483	0.000016	-45.6	4.3	2490	2606	-0.96
17XS-10-25	2189	0.031725	0.000653	0.281293	0.000015	-52.4	-4.4	2713	3066	-0.98
17XS-10-26	2666	0.011979	0.000264	0.281163	0.000015	-57.0	2.4	2859	2996	-0.99
17XS-10-27	2661	0.027651	0.000609	0.281116	0.000013	-58.6	0.0	2948	3147	-0.98
17XS-10-28	2173	0.036259	0.000733	0.281530	0.000014	-44.0	3.5	2397	2548	-0.98
17XS-10-29	2329	0.108632	0.002261	0.281431	0.000014	-47.5	1.1	2636	2824	-0.93
17XS-10-30	2285	0.034605	0.000696	0.281341	0.000016	-50.7	-0.6	2651	2899	-0.98
17XS-10-32	2179	0.066747	0.001314	0.281582	0.000015	-42.2	4.6	2362	2481	-0.96
17XS-10-33	2315	0.068022	0.001461	0.281328	0.000020	-51.1	-1.6	2723	2986	-0.96
17XS-10-34	2305	0.046406	0.001111	0.281408	0.000015	-48.3	1.6	2588	2775	-0.97
17XS-10-35	2498	0.037207	0.000754	0.281299	0.000017	-52.2	2.6	2712	2859	-0.98
17XS-10-36	2202	0.043223	0.000894	0.281660	0.000015	-39.4	8.5	2229	2248	-0.97
17XS-10-37	2172	0.044592	0.000915	0.281346	0.000015	-50.5	-3.3	2660	2983	-0.97
17XS-10-39	2331	0.038171	0.000862	0.281402	0.000016	-48.5	2.3	2580	2747	-0.97
17XS-10-41	2233	0.048142	0.001088	0.281329	0.000016	-51.1	-2.8	2695	2999	-0.97
17XS-10-42	2247	0.041536	0.000909	0.281337	0.000015	-50.8	-2.0	2672	2955	-0.97
17XS-10-43	2280	0.021951	0.000484	0.281229	0.000014	-54.6	-4.4	2787	3135	-0.99
17XS-10-44	2287	0.048479	0.001079	0.281435	0.000011	-47.4	2.1	2549	2723	-0.97
17XS-10-46	2288	0.042647	0.000927	0.281392	0.000014	-48.9	0.9	2598	2805	-0.97
17XS-10-47	2313	0.029831	0.000660	0.281195	0.000015	-55.8	-5.1	2845	3206	-0.98
17XS-10-48	2173	0.168269	0.003291	0.281484	0.000020	-45.6	-1.9	2634	2891	-0.90
17XS-10-49	2346	0.036313	0.000778	0.281309	0.000016	-51.8	-0.5	2700	2939	-0.98
17XS-10-50	2321	0.050359	0.001088	0.281207	0.000016	-55.4	-5.2	2862	3218	-0.97
17XS-10-51	2331	0.036881	0.000823	0.281412	0.000016	-48.2	2.7	2563	2719	-0.98
17XS-10-52	2192	0.055892	0.001187	0.281535	0.000015	-43.8	3.4	2419	2567	-0.96
17XS-10-53	2209	0.048900	0.001067	0.281525	0.000016	-44.2	3.6	2425	2567	-0.97
17XS-10-54	2339	0.043497	0.000921	0.281312	0.000014	-51.7	-0.8	2706	2952	-0.97
17XS-10-56	2326	0.091384	0.001865	0.281400	0.000015	-48.6	0.5	2651	2856	-0.94
17XS-10-58	2548	0.020626	0.000469	0.281424	0.000013	-47.7	8.6	2524	2507	-0.99
17XS-10-59	2298	0.048590	0.001015	0.281243	0.000014	-54.2	-4.3	2807	3145	-0.97
17XS-10-60	2522	0.026641	0.000568	0.281299	0.000013	-52.2	3.4	2699	2822	-0.98
17XS-10-61	2300	0.038331	0.000814	0.281359	0.000012	-50.1	0.1	2635	2861	-0.98
17XS-10-62	2316	0.025582	0.000532	0.281366	0.000014	-49.8	1.2	2606	2805	-0.98
17XS-10-64	2305	0.067137	0.001484	0.281322	0.000014	-51.3	-2.1	2732	3006	-0.96
17XS-10-65	2681	0.025606	0.000590	0.281097	0.000014	-59.3	-0.2	2972	3174	-0.98
17XS-10-66	2144	0.043663	0.000902	0.281570	0.000015	-42.6	4.0	2353	2492	-0.97
17XS-10-68	2291	0.047417	0.001028	0.281250	0.000016	-53.9	-4.2	2798	3133	-0.97
17XS-10-69	2291	0.049254	0.001065	0.281318	0.000013	-51.5	-1.9	2707	2982	-0.97
17XS-10-70	2266	0.023247	0.000534	0.281328	0.000014	-51.1	-1.3	2657	2924	-0.98
17XS-10-71	2269	0.041398	0.000918	0.281184	0.000016	-56.2	-6.9	2880	3286	-0.97
17XS-10-72	2126	0.018454	0.000370	0.281413	0.000014	-48.1	-1.2	2532	2811	-0.99
17XS-10-73	2285	0.029165	0.000606	0.281437	0.000012	-47.3	2.9	2515	2673	-0.98
17XS-10-74	2272	0.020594	0.000497	0.281321	0.000012	-51.4	-1.3	2665	2934	-0.99
17XS-10-75	2876	0.046347	0.001037	0.281030	0.000014	-61.7	1.0	3098	3250	-0.97
17XS-10-77	2235	0.019811	0.000448	0.281203	0.000014	-55.5	-6.3	2819	3219	-0.99
17XS-10-78	2800	0.026304	0.000558	0.281253	0.000012	-53.8	8.1	2760	2733	-0.98
17XS-10-79	2100	0.021899	0.000501	0.281259	0.000015	-53.6	-7.4	2748	3187	-0.98
17XS-19-01	2099	0.048845	0.000925	0.281544	0.000014	-43.5	2.1	2389	2581	-0.97
17XS-19-02	2094	0.038001	0.000725	0.281507	0.000014	-44.8	0.9	2428	2652	-0.98
17XS-19-03	2106	0.060253	0.001214	0.281463	0.000014	-46.4	-1.1	2519	2788	-0.96
17XS-19-05	1866	0.041524	0.000842	0.281516	0.000013	-44.5	-4.0	2423	2788	-0.97
17XS-19-06	2067	0.005608	0.000133	0.281453	0.000012	-46.7	-0.8	2463	2739	-1.00
17XS-19-07	2254	0.027553	0.000589	0.281377	0.000017	-49.4	0.1	2595	2828	-0.98
17XS-19-09	2102	0.021427	0.000474	0.281585	0.000013	-42.0	4.3	2306	2445	-0.99
17XS-19-10	2056	0.028562	0.000562	0.281404	0.000016	-48.5	-3.4	2557	2896	-0.98
17XS-19-11	2583	0.062470	0.001244	0.281172	0.000013	-56.7	-0.9	2921	3145	-0.96
17XS-19-12	2063	0.031394	0.000611	0.281484	0.000014	-45.6	-0.4	2451	2714	-0.98
17XS-19-14	2222	0.028366	0.000601	0.281282	0.000012	-52.8	-4.0	2724	3065	-0.98

(continued on next page)

Table 2 (continued)

Spot no.	Age (Ma)	$^{176}\text{Yb}/^{177}\text{Hf}$	$^{176}\text{Lu}/^{177}\text{Hf}$	$^{176}\text{Hf}/^{177}\text{Hf}$	2σ	$\epsilon_{\text{Hf}}(0)$	$\epsilon_{\text{Hf}}(t)$	T_{DM1} (Ma)	T_{DM}^{c} (Ma)	$f_{\text{Lu/Hf}}$
17XS-19-15	2087	0.068122	0.001364	0.281432	0.000011	-47.5	-2.8	2573	2884	-0.96
17XS-19-16	2194	0.022350	0.000478	0.281281	0.000013	-52.8	-4.5	2717	3074	-0.99
17XS-19-17	2065	0.054363	0.001059	0.281467	0.000014	-46.2	-1.6	2503	2790	-0.97
17XS-19-18	2237	0.025137	0.000571	0.281416	0.000014	-48.0	1.1	2541	2749	-0.98
17XS-19-19	2203	0.071326	0.001363	0.281428	0.000016	-47.6	-0.4	2577	2818	-0.96
17XS-19-20	2195	0.048048	0.000957	0.281513	0.000014	-44.6	3.1	2434	2592	-0.97
17XS-19-21	2200	0.037262	0.000710	0.281415	0.000014	-48.1	0.1	2552	2789	-0.98
17XS-19-22	2113	0.050987	0.001357	0.281463	0.000013	-46.4	-1.1	2529	2796	-0.96
17XS-19-23	2115	0.038540	0.000778	0.281416	0.000012	-48.0	-1.9	2555	2850	-0.98
17XS-19-26	2184	0.041856	0.000928	0.281453	0.000013	-46.7	0.7	2514	2733	-0.97
17XS-19-28	2077	0.066336	0.001339	0.281675	0.000011	-38.9	5.7	2235	2336	-0.96
17XS-19-29	2324	0.038733	0.000765	0.281397	0.000011	-48.7	2.1	2580	2752	-0.98
17XS-19-30	2350	0.131126	0.002318	0.281583	0.000023	-42.1	6.8	2425	2470	-0.93
17XS-19-32	2180	0.132348	0.002504	0.281605	0.000012	-41.3	3.7	2405	2539	-0.92
17XS-19-33	2102	0.069381	0.001351	0.281706	0.000013	-37.8	7.3	2192	2250	-0.96
17XS-19-35	2115	0.041406	0.000867	0.281441	0.000014	-47.2	-1.2	2527	2801	-0.97
17XS-19-36	2198	0.033507	0.000826	0.281439	0.000012	-47.2	0.7	2527	2746	-0.98
17XS-19-37	2198	0.044453	0.000916	0.281339	0.000017	-50.7	-3.0	2669	2982	-0.97
17XS-19-38	2339	0.033452	0.000667	0.281273	0.000015	-53.1	-1.8	2741	3015	-0.98
17XS-19-39	2331	0.043215	0.000858	0.281436	0.000015	-47.3	3.5	2532	2668	-0.97
17XS-19-40	2291	0.047819	0.000981	0.281361	0.000015	-50.0	-0.2	2644	2878	-0.97
17XS-19-43	2173	0.059234	0.001186	0.281471	0.000013	-46.1	0.7	2506	2724	-0.96
17XS-19-44	2158	0.031896	0.000634	0.281524	0.000012	-44.2	3.1	2399	2562	-0.98
17XS-19-45	2061	0.089110	0.002111	0.281551	0.000015	-43.3	-0.2	2457	2697	-0.94
17XS-19-46	2176	0.034118	0.000698	0.281480	0.000012	-45.8	1.8	2463	2657	-0.98
17XS-19-47	2090	0.008744	0.000177	0.281471	0.000013	-46.1	0.4	2441	2685	-0.99
17XS-19-48	2676	0.020169	0.000440	0.281147	0.000014	-57.5	1.8	2894	3047	-0.99
17XS-19-49	2174	0.037910	0.000788	0.281476	0.000012	-45.9	1.5	2473	2674	-0.98
17XS-19-51	2035	0.022844	0.000402	0.281470	0.000017	-46.1	-1.3	2457	2746	-0.99
17XS-19-52	2146	0.023164	0.000617	0.281472	0.000014	-46.0	1.0	2468	2686	-0.98
17XS-19-54	2299	0.016803	0.000439	0.281321	0.000015	-51.4	-0.6	2660	2910	-0.99
17XS-19-55	2311	0.021393	0.000492	0.281314	0.000017	-51.6	-0.7	2673	2922	-0.99
17XS-19-56	1989	0.064907	0.001538	0.281688	0.000014	-38.4	3.9	2228	2379	-0.95
17XS-19-58	2284	0.027934	0.000576	0.281248	0.000013	-54.0	-3.8	2768	3098	-0.98
17XS-19-60	2165	0.077061	0.001622	0.281480	0.000015	-45.8	0.2	2523	2750	-0.95
17XS-19-64	2318	0.032237	0.000786	0.281320	0.000014	-51.4	-0.8	2685	2933	-0.98
17XS-19-67	2239	0.031234	0.000738	0.281311	0.000012	-51.8	-2.8	2695	3002	-0.98
17XS-19-68	2132	0.049193	0.001032	0.281358	0.000015	-50.1	-3.9	2651	2992	-0.97
17XS-19-69	2265	0.087019	0.001807	0.281281	0.000016	-52.8	-4.9	2812	3155	-0.95
17XS-19-70	1987	0.050344	0.000947	0.281572	0.000013	-42.5	0.5	2353	2594	-0.97
17XS-19-73	2122	0.037917	0.000752	0.281379	0.000012	-49.3	-3.0	2603	2924	-0.98
17XS-19-76	1970	0.025564	0.000540	0.281458	0.000013	-46.5	-3.3	2483	2828	-0.98
17XS-19-77	2313	0.022745	0.000524	0.281349	0.000016	-50.4	0.6	2628	2845	-0.98
17XS-19-78	2220	0.032561	0.000874	0.281450	0.000013	-46.8	1.5	2515	2711	-0.97
17XS-19-79	2140	0.059580	0.001118	0.281557	0.000013	-43.0	3.2	2384	2544	-0.97
17XS-19-81	2184	0.032051	0.000665	0.281470	0.000014	-46.1	1.7	2475	2672	-0.98
17XS-19-84	2289	0.026886	0.000584	0.281182	0.000015	-56.3	-6.0	2857	3244	-0.98
17XS-19-85	2298	0.043472	0.000938	0.281336	0.000012	-50.9	-0.9	2675	2926	-0.97

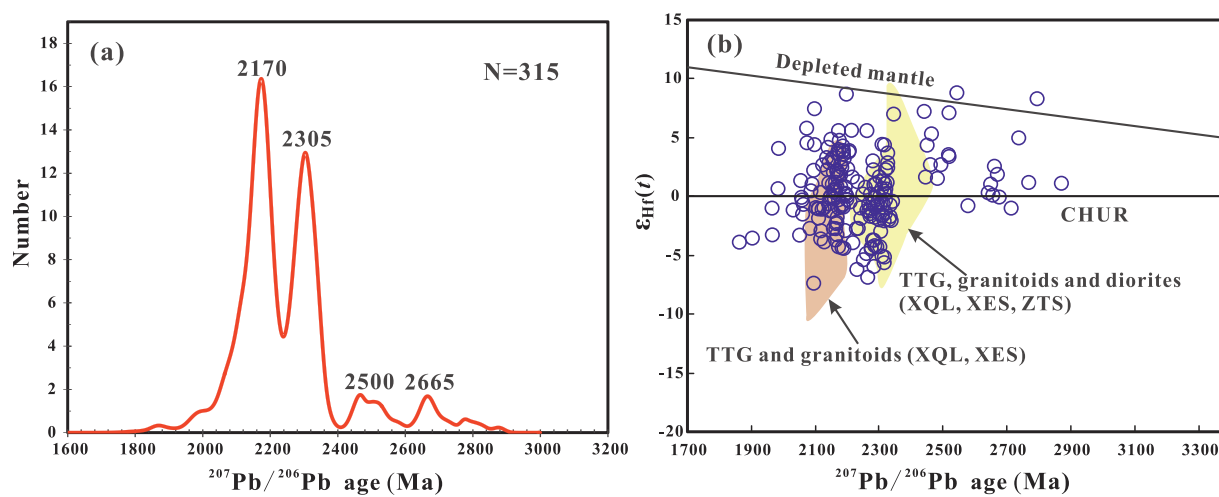


Fig. 6. (a) Age distributions of all analyzed detrital zircons from Fangniushan metasedimentary rocks and (b) $\epsilon_{\text{Hf}}(t)$ vs. $^{207}\text{Pb}/^{206}\text{Pb}$ ages diagram of all analyzed detrital zircons.

Table 3

Major and trace element data of the Fangniushan metasedimentary rocks in the Xiaoshan area.

Sample no.	18XS-1	18XS-2	17XS-1	17XS-2	17XS-4	17XS-6	17XS-7	17XS-9	17XS-10	17XS-11	17XS-12	17XS-16	17XS-17	17XS-22	17XS-24
Major oxides (wt.%)															
SiO ₂	81.85	87.70	88.54	96.88	91.82	90.59	86.07	88.46	88.42	70.32	87.86	78.38	83.63	69.61	67.51
TiO ₂	0.24	0.06	0.13	0.04	0.03	0.02	0.12	0.08	0.06	0.08	0.04	0.19	0.24	0.39	0.27
Al ₂ O ₃	11.02	7.64	6.02	1.29	4.41	5.12	8.08	6.52	7.01	14.83	7.21	10.06	9.15	16.97	15.04
Fe ₂ O ₃ T	1.55	1.04	1.71	0.93	1.40	1.23	1.33	1.22	1.26	1.53	1.25	2.25	1.97	0.64	2.33
MnO	0.04	0.04	0.08	0.06	0.06	0.07	0.07	0.07	0.06	0.12	0.07	0.09	0.05	0.04	0.06
MgO	0.12	0.08	0.11	0.06	0.13	0.10	0.08	0.07	0.10	0.20	0.10	0.79	0.14	0.22	1.78
CaO	0.10	0.04	0.10	0.03	0.04	0.08	0.08	0.07	0.07	2.88	0.04	1.23	0.14	1.98	2.94
Na ₂ O	0.21	0.18	0.13	0.01	0.09	0.11	0.17	0.13	0.14	3.18	0.14	0.12	0.20	7.01	4.58
K ₂ O	3.13	2.13	1.69	0.44	1.23	1.46	2.28	1.80	2.00	3.09	2.07	3.21	2.48	1.36	2.16
P ₂ O ₅	0.07	0.02	0.08	0.01	0.02	0.02	0.06	0.05	0.02	0.03	0.02	0.10	0.13	0.15	0.13
L.O.I	1.58	0.99	1.00	0.29	0.92	0.75	1.23	0.91	0.91	3.73	0.84	2.92	1.41	1.55	3.03
Total	17.82	12.16	10.92	3.12	8.30	8.94	13.38	10.84	11.57	29.59	11.74	20.77	15.67	29.92	32.05
Trace elements (ppm)															
Sc	2.70	1.50	3.00	0.90	2.20	0.80	2.10	2.10	1.00	1.20	1.10	7.80	2.50	8.60	2.10
Ti	0.11	0.04	0.05	0.02	0.02	0.01	0.05	0.03	0.03	0.06	0.03	0.08	0.08	0.22	0.16
V	13.00	4.00	14.00	7.00	7.00	5.00	9.00	10.00	6.00	8.00	5.00	29.00	20.00	44.00	29.00
Cr	18.00	50.00	21.00	31.00	19.00	70.00	20.00	20.00	69.00	10.00	20.00	19.00	67.00	20.00	49.00
Co	1.20	1.00	2.40	0.90	1.10	1.20	1.70	1.70	1.40	0.90	1.20	3.90	3.10	0.50	3.20
Ni	4.10	2.50	3.80	2.00	1.70	3.10	2.30	2.60	2.70	0.50	2.20	7.40	3.60	1.20	12.60
Ga	11.75	7.99	7.89	2.21	5.26	5.64	9.70	7.01	7.40	16.90	8.10	12.70	10.85	14.60	18.55
Ge	0.10	0.07	0.12	0.06	0.05	0.05	0.09	0.09	0.06	0.09	0.11	0.25	0.21	0.42	0.32
Rb	109.00	74.40	54.70	13.90	40.50	48.90	72.00	56.60	66.30	90.40	66.60	116.00	93.10	57.80	77.50
Sr	55.40	44.20	32.40	2.80	17.90	22.60	38.00	32.40	30.40	311.00	32.50	54.80	84.10	234.00	290.00
Ba	810.00	570.00	601.00	53.10	274.00	367.00	535.00	707.00	567.00	1040.00	495.00	926.00	693.00	178.50	563.00
Y	20.10	6.60	14.20	2.20	14.60	4.10	11.70	12.00	7.50	8.10	6.80	25.30	16.50	12.90	4.70
Nb	6.00	1.80	6.20	1.40	1.80	1.20	5.10	3.80	3.20	8.60	2.40	7.30	10.50	10.20	6.10
Ta	1.00	0.30	0.50	0.11	0.11	0.08	0.32	0.17	0.18	0.33	0.15	0.34	0.68	0.85	0.41
Zr	324.00	106.00	174.00	40.00	58.00	62.00	169.00	109.00	97.00	101.00	90.00	173.00	124.00	178.00	135.00
Hf	9.10	3.00	5.00	1.20	1.80	1.90	4.70	3.10	2.70	3.10	2.70	4.70	3.60	4.70	3.50
Pb	8.80	2.00	3.90	1.10	2.80	2.00	3.10	3.60	2.60	26.60	2.60	10.20	5.80	4.00	4.80
Th	12.35	6.19	19.10	2.94	6.14	4.09	12.30	9.08	6.39	1.33	7.13	17.50	30.60	9.51	6.86
U	1.51	0.57	1.38	0.70	0.66	0.60	0.91	0.83	0.80	1.27	0.62	2.58	4.00	1.24	0.91
La	32.80	13.20	42.70	4.00	16.10	11.40	28.70	24.70	18.00	8.20	18.20	65.50	83.70	140.00	31.10
Ce	64.00	25.00	82.70	7.30	33.80	21.80	54.60	49.00	34.70	15.80	35.80	122.00	152.50	278.00	60.60
Pr	7.29	2.89	7.97	0.71	3.04	2.09	5.53	4.97	3.47	1.63	3.46	12.20	15.30	26.90	5.85
Nd	26.00	10.00	26.90	2.50	11.40	7.20	19.00	16.90	11.10	5.70	12.00	42.40	50.10	87.20	19.00
Sm	4.39	1.53	3.99	0.47	2.25	1.04	2.47	2.72	1.80	1.19	1.98	6.45	6.63	11.85	2.45
Eu	0.95	0.24	0.61	0.09	0.40	0.17	0.39	0.45	0.28	0.39	0.30	1.40	0.96	2.35	0.66
Gd	3.89	1.14	3.04	0.36	2.37	0.89	1.79	2.40	1.52	1.08	1.41	5.24	4.37	6.91	1.73
Tb	0.62	0.17	0.45	0.06	0.37	0.13	0.32	0.34	0.23	0.18	0.20	0.71	0.57	0.71	0.17
Dy	3.73	1.04	2.51	0.35	2.28	0.74	2.02	2.22	1.40	1.09	1.24	4.11	3.06	3.06	0.88
Ho	0.74	0.23	0.51	0.07	0.48	0.15	0.43	0.48	0.27	0.26	0.26	0.80	0.62	0.45	0.16
Er	2.15	0.70	1.48	0.20	1.41	0.44	1.24	1.36	0.75	0.83	0.78	2.36	1.78	1.12	0.44
Tm	0.32	0.11	0.23	0.03	0.21	0.07	0.19	0.20	0.11	0.14	0.12	0.36	0.26	0.15	0.06
Yb	2.11	0.76	1.56	0.22	1.38	0.45	1.21	1.32	0.76	1.07	0.76	2.27	1.68	0.87	0.34
Lu	0.32	0.13	0.23	0.04	0.21	0.07	0.19	0.20	0.12	0.18	0.12	0.34	0.24	0.12	0.05
REE	149.31	57.14	174.88	16.40	75.70	46.64	118.08	107.26	74.51	37.74	76.63	266.14	321.77	559.69	123.49
Eu/Eu*	0.69	0.53	0.51	0.64	0.53	0.53	0.54	0.53	0.50	1.03	0.52	0.71	0.51	0.73	0.93
La/Yb	11.15	12.46	19.63	13.04	8.37	18.17	17.01	13.42	16.99	5.50	17.18	20.70	35.74	115.43	65.61
Gd/Yb	1.53	1.24	1.61	1.35	1.42	1.64	1.22	1.50	1.65	0.83	1.53	1.91	2.15	6.57	4.21

normalized REE patterns (Fig. 8b) (Rudnick and Gao, 2003).

5. Discussion

5.1. Depositional age of the Fangniushan supracrustal strata

Although the Fangniushan supracrustal strata was thought to be formed in Paleoproterozoic based on stratigraphic correlation with both underlying and overlying units (BGMRHP, 1995), the depositional age of this strata have not been well constrained because of its lack of reliable geochronological data. However, due to the lack of biological fossils and interlayered volcanic rocks in Precambrian sedimentary sequences, it is very difficult to obtain a precise estimation of the depositional age. Detrital zircon, a mechanically robust mineral, on the other hand, can survive erosion, transportation, diagenesis and metamorphism, and effectively constrain the maximum depositional age of a sedimentary sequence (e.g. Fedo et al., 2003, Wang et al., 2017b, 2018a,b; Liu et al., 2016, 2018).

Detrital zircon grains from different samples of the Fangniushan supracrustal strata display obvious oscillatory growth zonings and high Th/U values (0.64 on average), suggesting a magmatic origin (Vavra et al., 1999; Hoskin and Black, 2000). Furthermore, the metasedimentary rocks only experienced low greenschist facies metamorphism, which precludes the possibility of metamorphic resetting or recrystallization after deposition. Detrital zircons in this study yield wide $^{207}\text{Pb}/^{206}\text{Pb}$ ages ranging from 1.83 Ga to 2.88 Ga with the majority older than 2.0 Ga. The youngest concordant $^{207}\text{Pb}/^{206}\text{Pb}$ age group define a weighted average age of 1873 ± 32 Ma ($n = 3$, MSWD = 0.92), older than the single-grain youngest age of 1833 ± 50 Ma found in sample 17XS-5. We prefer to use the ~ 1.87 Ga to represent the maximum depositional age as it was suggested that the reliable age constraint should belong to a significant population composed of three or more zircons (Andersen, 2005). Additionally, the Fangniushan supracrustal strata is unconformably overlain by the Xiong'er Group. SHRIMP and LA-ICP-MS U-Pb analyses on magmatic zircons from the Xiong'er volcanic rocks reveal that the Xiong'er Group

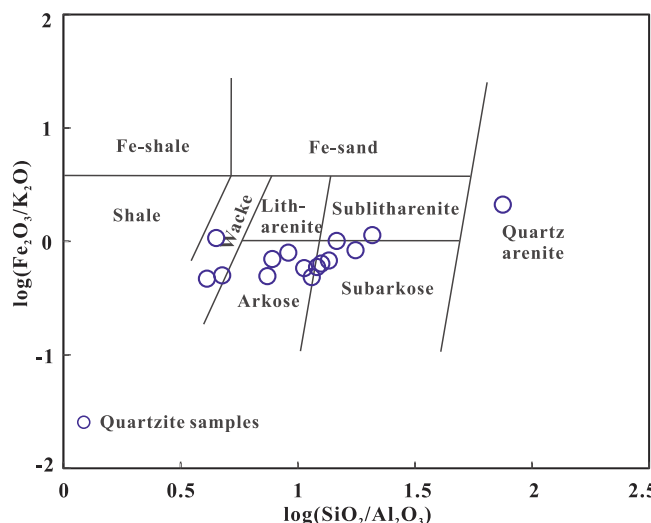


Fig. 7. Classification for samples of Fangniushan supracrustal strata after Herron (1988) using $\log(\text{Fe}_2\text{O}_3/\text{K}_2\text{O})$ vs. $\log(\text{SiO}_2/\text{Al}_2\text{O}_3)$.

was formed at 1.80–1.75 Ga (Zhao et al., 2002, 2004b; Peng et al., 2008; He et al., 2009; Zhao et al., 2009; Wang et al., 2010), which can be used to constrain the minimum depositional age of the Fangniushan supracrustal strata.

In summary, based on our new geochronological data and those from other studies, we propose that the Fangniushan supracrustal strata were formed at the time between ~1.87 Ga and ~1.80 Ga, which is consistent with the depositional time of the Tietonggou Formation in the adjacent Xiaoqinling area (1.91–1.80 Ga, Diwu et al., 2013).

5.2. Sedimentary provenance

5.2.1. Source-area chemical weathering and maturity

Geochemistry characteristics of clastic sedimentary rocks are powerful tools to trace the provenance (Cox et al., 1995; Hofmann, 2005; Sugitani et al., 2006). Chemical compositions of sedimentary rocks, however, could be modified by sedimentary processes and metamorphism, including transportation, deposition, diagenesis, post-depositional chemical weathering and alteration (Taylor and McLennan, 1985; Roddaz et al., 2006; Wang et al., 2018a). Therefore, it is necessary to evaluate the influence of these processes on the chemical compositions of sediments (e.g. Wang and Zhou, 2013).

The composition of source rocks and weathering trend can be illustrated by the A (Al_2O_3)–CN ($\text{CaO}^* + \text{Na}_2\text{O}$)–K (K_2O) triangular

diagram of molecular proportions, where CaO^* refers to CaO present in silicate minerals (Nesbitt and Young, 1984, 1989). On the A-CN-K diagram (Fig. 9a), the Fangniushan metasedimentary rocks are mainly plotted along the weathering trend predicted by the average A-type granite line composition, indicating the provenance underwent low degree of chemical weathering and do not affected by post-depositional alteration of potassium (K). This conclusion is also supported by the Chemical Index of Alteration (CIA) principle proposed by Fedo et al. (1995), which is frequently used to evaluate the degree of chemical weathering in the source of sedimentary rocks. CIA values of all samples are lower than that of Post Archean Australian Shale (PAAS = 70–75; McLennan et al., 1993) (Fig. 9b), indicating generally weak to moderate weathering on the Fangniushan metasedimentary rocks.

$\text{SiO}_2/\text{Al}_2\text{O}_3$ is a commonly used index for evaluating compositional maturation of sediments (Roser and Korsch, 1986), with more quartz and less feldspar and mafic minerals, maturity as well as $\text{SiO}_2/\text{Al}_2\text{O}_3$ ratios in sediments become higher. All the $\text{SiO}_2/\text{Al}_2\text{O}_3$ ratios of the studied samples are higher than 4.0 (4.1–75.1), suggesting that the detritus underwent long term recycling before accumulation and have higher level of maturity. In addition, the maturity of the clastic sedimentary rocks can be reflected by the Index of Compositional Variability (ICV) values (Cox et al., 1995). Typically, sediments with low ICV values may have been derived from a mature source containing large amounts of clay minerals, indicating sediment recycling in a passive tectonic setting (Van de Kamp and Leake, 1985). By contrast, sediments with high ICV values could imply first cycle deposits sourced from immature rocks in an active tectonic environment (Van de Kamp and Leake, 1985). The ICV values of the Fangniushan metasedimentary rocks range from 0.48 to 1.46 (Fig. 9b), suggesting the sedimentary protoliths were mainly derived from a chemically mature sedimentary source, with minor contribution from immature source (Fedo et al., 1995; Cox et al., 1995).

5.2.2. Nature of source rocks

Concentrations and patterns of REEs have been utilized as reliable indicators for sedimentary provenance (Taylor and McLennan, 1985). Although the samples from the Fangniushan metasedimentary rocks have varied total REE concentrations, they show similar chondrite-normalized REE patterns, with LREE enrichments, relatively flat HREE and slightly negative Eu anomalies, indicating felsic to intermediate dominant sedimentary provenance (Slack and Stevens, 1994; Wang et al., 2012).

Trace elements, such as La, Th, Zr, Hf, Co and Sc, have been proven to be useful tools for discriminating felsic and mafic materials as they have relatively low mobility during post-depositional alterations (Taylor and McLennan, 1985; Bhatia and Crook, 1986; Cullers, 2000).

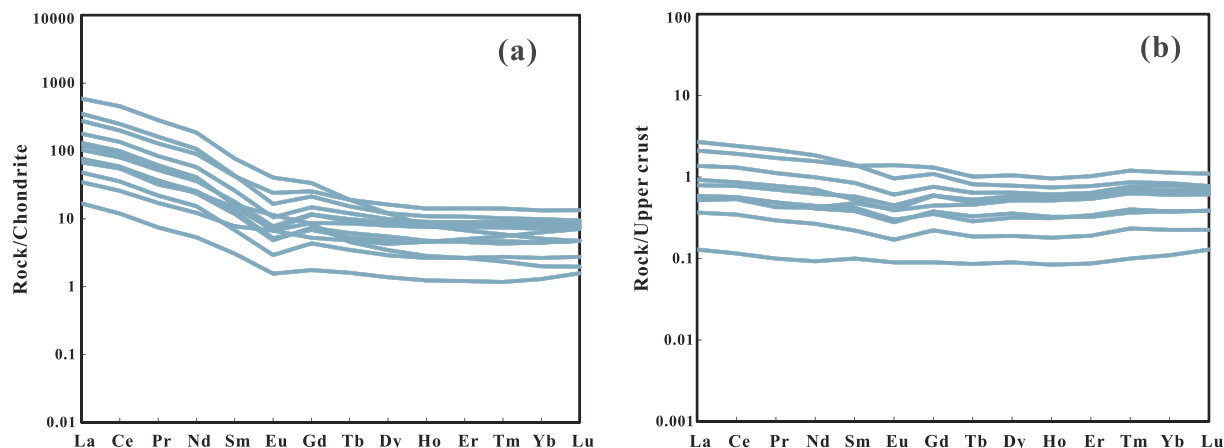


Fig. 8. Chondrite-and upper crust-normalized REE patterns for samples of Fangniushan supracrustal strata. Chondrite and upper crust-normalized data after Sun and McDonough (1989) and Rudnick and Gao (2003).

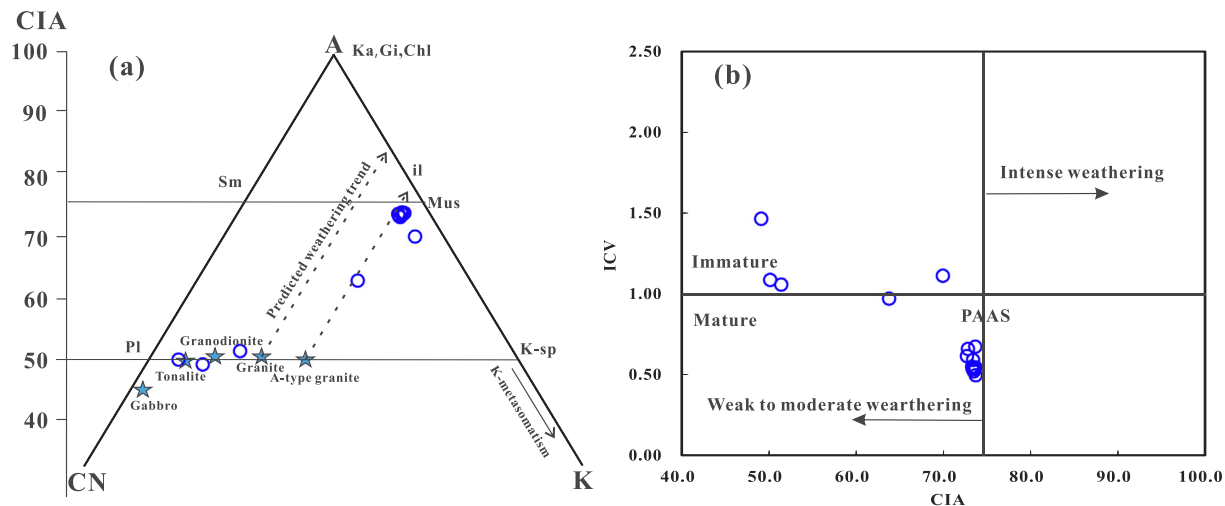


Fig. 9. Geochemical diagrams showing variations of weathering and maturity for Fangniushan supracrustal strata. (a) A-CN-K diagram after Nesbitt and Young (1984). Abbreviations for Ka: kaolinite, Gi: gibbsite, Chl: chlorite, Sm: smectite, il: illite, Mus: muscovite, Pl: plagioclase, K-sp: potassium plagioclase; (b) CIA-ICV diagram after Nesbitt and Young (1982). Symbols are the same as in Fig. 7.

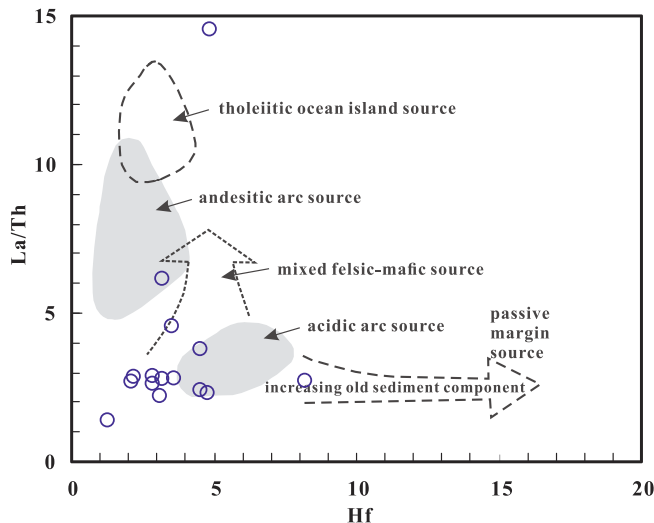


Fig. 10. La/Th-Hf diagram showing source compositions for Fangniushan supracrustal strata (after Floyd and Leveridge, 1987). Symbols are the same as in Fig. 7.

The metasedimentary rocks of the present study have low Cr/Zr and Cr/Th values of 0.06–1.13 and 1.09–17.11, respectively; and high Th/Cr (0.06–0.92), Th/Sc (1.11–12.24), La/Sc (4.44–33.48), and La/Co (4.44–280), comparable with those of felsic rocks and upper continental crust (Taylor and McLennan, 1985; Cullers, 2000). Also, Floyd and Leveridge (1987) used a La/Th vs. Hf plot to discriminate different source compositions for sandstones. In Fig. 10, the majority of samples fall in the field of acidic arc source fields, indicating that the source materials were dominated of felsic rocks. In the ternary diagrams of La-Th-Sc and Th-Hf-Co (Fig. 11a, b), most samples cluster near the compositions of granite components, indicating a felsic signature of source rocks, in agreement with the interpretation from REE features as discussed above.

In addition, on the A-CN-K triangular plot (Fig. 9a), the weathering trends of the majority studied samples are parallel to the average A-type granite line composition, reflecting an acid rock source. Therefore, we conclude that the Fangniushan metasedimentary rocks dominantly received detritus from felsic sources composed of TTG-like, granitic, and felsic volcanic rocks.

5.2.3. Possible source areas

Detrital zircon U-Pb ages combined with whole-rock geochemistry and zircon Hf isotopes of sedimentary rocks can provide useful information about their potential provenance (e.g. Roser and Korsch, 1986; McLennan et al., 1993; Fedo et al., 2003; Sun et al., 2017a; Liu et al., 2017, 2018; Wang et al., 2012, 2018a,b). All of the detrital zircons from the Fangniushan metasedimentary rocks yield magmatic ages of 1833–2876 Ma, and can be divided into three groups: ~2.00–2.24 Ga, ~2.25–2.40 Ga and ~2.50–2.88 Ga, peaking at 2.17 Ga, 2.31 Ga and 2.50–2.67 Ga, respectively (Fig. 6a). In comparison with the latter two groups, the ~2.00–2.24 Ga detrital zircons (54%) are predominant in the Fangniushan metasedimentary rocks. The zircon populations at ~2.00–2.24 Ga are consistent with the ages of 2.16 Ga Bayuan tonalite gneiss in the Xiaoqinling area (Huang et al., 2013), the 2.06–2.19 Ga Ganshugou tonalite and K-feldspar granite gneiss (Huang et al., 2012), and the 2.16–2.17 Ga Muce monzonitic gneisses (Chen et al., 2016) in the Xiong'ershan area. Additionally, these igneous rocks yield a wide range of zircon $\epsilon_{\text{Hf}}(t)$ values, which overlap with those of the 2.00–2.24 Ga detrital zircons (−7.3 to +8.9) from the studied samples (Fig. 6b). Therefore, these ~2.00 to 2.24 Ga zircons are likely to be derived from the coeval igneous rocks in the adjacent Xiaoqinling and Xiong'ershan areas.

The subordinate population (34%) of detrital zircons has the age range between 2.25 Ga and 2.40 Ga, with age peak at ~2.31 Ga. Magmatic events of this period were widely recognized in the southern NCC, adjacent possible provenance include the 2.31–2.32 Ga TTG gneisses, quartz diorites (Diwu et al., 2018), and 2.34 Ga granitoid gneisses (Luo, 2016) in the Xiaoshan area. The 2.25–2.32 Ga TTG gneisses (Huang et al., 2013; Diwu et al., 2014; Wang et al., 2017a) and 2.29–2.36 Ga granitoids (Huang et al., 2013; Yu et al., 2013; Diwu et al., 2014; Wang et al., 2017a) in the Xiaoqinling area. The 2.31–2.34 Ga TTG gneisses (Diwu et al., 2007; Huang et al., 2012) and 2.30–2.31 Ga diorites (Huang et al., 2012; Diwu et al., 2014; Zhou et al., 2016) in the Xiong'ershan area. The 2.35 Ga granites (Zhang et al., 2012) in the Zhongtiaoshan area. Besides, $\epsilon_{\text{Hf}}(t)$ values of the 2.25–2.40 Ga detrital zircons (−6.9 to +6.8) are identical with the similar-aged zircons found in the Xiaoshan and adjacent Xiaoqinling, Xiong'ershan and Zhongtiaoshan areas (Fig. 6b). Such geochronological and isotopic similarities suggest that the detrital zircons age at 2.25–2.40 Ga were sourced from the coeval igneous rocks in the southern NCC.

The 2.50–2.88 Ga detrital zircons are documented in all the four samples but only make up 12% of all the zircon ages, although

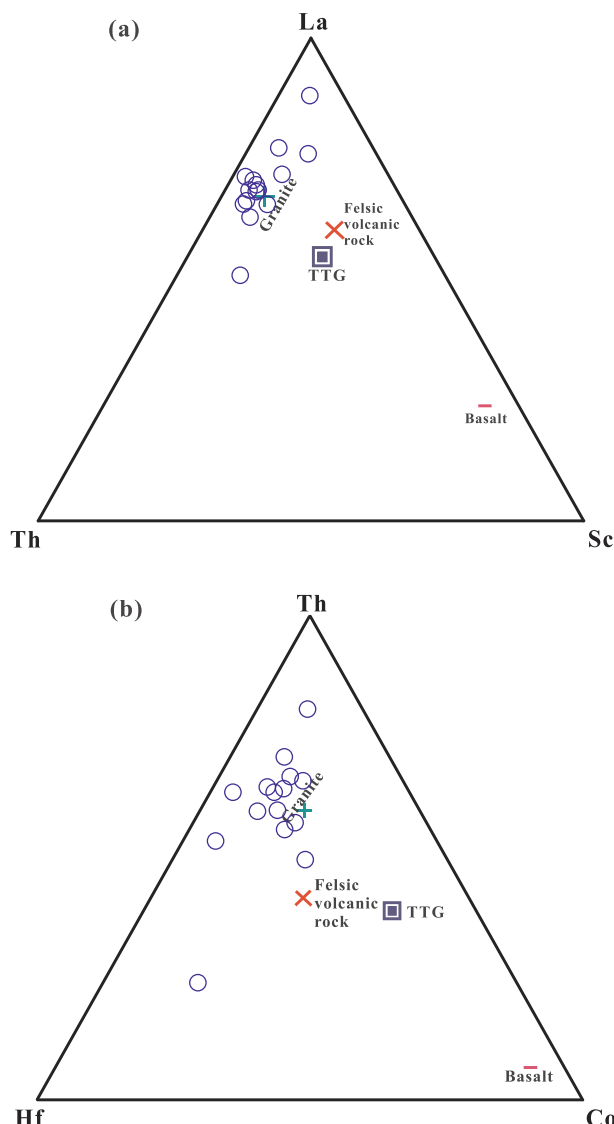


Fig. 11. Geochemical triangle diagrams of sedimentary samples from the Fangniushan supracrustal strata. (a) La-Th-Sc diagram after Cullers and Podkorytov (2000); (b) Th-Hf-Co diagram after Wang et al., (2012). Average source rock compositions are from Condie (1993). Symbols are the same as in Fig. 7.

Neoarchean is the strongest crustal growth time of the southern NCC (Diwu et al., 2014; Sun et al., 2017a). Such an age range fits precisely with the 2.50–2.52 Ga TTG gneisses in the Xiaoshan area (Diwu et al., 2018; Luo et al., 2018). The 2.79–2.80 Ga TTG gneisses (Jia et al., 2016), 2.48–2.55 Ga TTG gneisses (Huang et al., 2013; Wang et al., 2017a), 2.47 Ga granitoid and diorite gneisses (Huang et al., 2013; Diwu et al., 2014) in the Xiaoqinling area. The 2.45–2.56 TTG gneisses (Sun and Hu, 1993; Tian et al., 2006; Guo et al., 2008; Zhang et al., 2013), 2.71 Ga TTG gneiss (Zhu et al., 2013), and 2.44–2.62 Ga granitoids (Yu et al., 2006; Zhao et al., 2012a; Zhang et al., 2012) in the Zhongtiaoshan area. We interpret the Neoarchean to early Paleoproterozoic felsic igneous rocks from these regions are the main sources for the 2.50–2.88 Ga detrital zircons in the Fangniushan metasedimentary rocks.

5.3. Depositional setting and implications for the Paleoproterozoic tectonic evolution of the southern NCC

As discussed in the preceding section, the tectonic evolution of the

NCC during the Paleoproterozoic is still under debate. The Fangniushan sedimentary sequence in the southern NCC shows a coarsening sequence from the base upwards (BGMRHP, 1995), which consists mainly of thick bedded meta-sandstones and conglomerates metamorphosed in the sub-greenschist facies, with cross-beddings in some quartzites, both of which are consistent with molasse deposits formed in a foreland basin (Condie, 1997). In addition, the Fangniushan metasedimentary rocks show wide range of detrital zircon ages from 1.86 Ga to 2.88 Ga, favor a foreland basin as sediments in foreland basin are likely to receive detritus from both cratonic interior and newly formed materials (DeCelles and Giles, 1996; Condie, 1997; Cawood et al., 2012). Moreover, the contemporary igneous rocks including granites and mafic dykes were formed mainly at ~1.86–1.80 Ga in the southern NCC, which were suggested resulted from partial melting of pre-existing crustal materials in a syn-orogenic or post-orogenic setting (e.g. Deng et al., 2016; Jia et al., 2016, 2020; Wang et al., 2017a). Combined with the late Palaeoproterozoic metamorphism of the southern NCC (Lu et al., 2020, and references therein), a collision-related foreland basin setting is reasonable for the Fangniushan supracrustal strata.

On the other hand, the typical tectonic environment (oceanic island arc, continental island arc, active continental margin and passive margin) of sandstones can be strongly reflected by their geochemical compositions (Bhatia, 1983; Bhatia and Crook, 1986; Mcleman and Taylor, 1991). Our new data indicate that the Paleoproterozoic Fangniushan metasedimentary rocks are relatively enriched in the LREE and depleted in the HREE, with negative Eu anomalies, relatively high La/Sc, La/Y, and low Sc/Cr values, suggesting they were deposited in a basin associated with plate convergence (Bhatia and Crook, 1986). Immobile elements, such as La, Th, Sc, and Zr, are widely used in distinguishing tectonic environments (Bhatia and Crook, 1986). On the frequently used Th-Zr/10-Co, Th-Sc-Zr/10 and La-Th-Sc diagrams for tectonic setting discrimination of sandstones (Bhatia and Crook, 1986), majority of the studied samples cluster in or around the continental island arc and passive continental margin field (Fig. 12), which is in strong agreement with those of retro-arc basins, as they contain both arc-related lithologies and craton-derived sources (DeGraaff-Surpless et al., 2002; Liu et al., 2012a; Wang et al., 2018b). Consequently, we suggest that the Fangniushan supracrustal strata in southern NCC was most likely formed in a retro-arc foreland environment in the period of 1.87–1.80 Ga.

Apart from the Fangniushan metasedimentary rocks in the Xiaoshan area, there are several Paleoproterozoic metavolcanic-sedimentary sequences deposited in the southern NCC, which can provide significant constraints on the Paleoproterozoic tectonic evolution. For example, the Yinyugou Group in the Wangwushan area and Songshan Group in the Dengfeng area were formed at the time after ~2.35 Ga, they show similar characteristics in terms of lithologies (mainly siliciclastics rocks), metamorphic grade (greenschist facies), and sedimentary

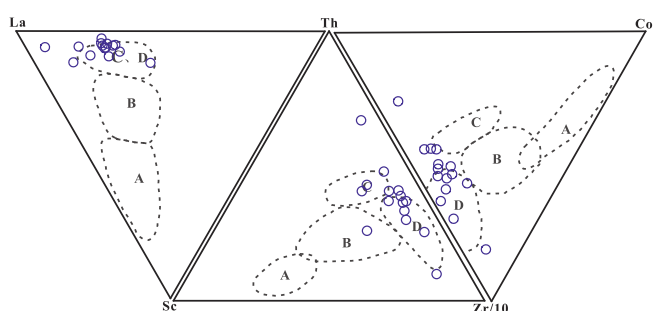


Fig. 12. La-Sc-Th, Th-Sc-Zr/10 and Th-Zr/10-Co plots of Fangniushan metasedimentary rocks for tectonic setting discrimination (after Bhatia and Crook, 1986). Dotted lines represent the dominant fields for the various tectonic settings: OIA-oceanic island arc; CIA-continental island arc; ACM-active continental margin; PM-passive margin. Symbols are the same as in Fig. 7.

environment (neritic-littoral facies clastics-carbonate formation) (Diwu et al., 2008; Liu et al., 2012a; Sun et al., 2017a). The Songshan Group was tentatively correlated with the Hutuo Group in the Wutai Complex, which were interpreted to deposit in a rift basin (Du et al., 2009, 2010, 2017; Wan et al., 2009). Recently, our new geochronological and geochemical data suggest that an extensional continental setting was most likely represented by the Yinyugou Group (Sun et al., 2017a). In addition, the ~2.23 to 2.13 Ga upper Taihua Group in the Lushan area show similar characteristics to the Khondalite Series (Sun, 1983; Wan et al., 2006; Diwu et al., 2010; Sun et al., 2017b), which has long been considered to deposited in a stable continental margin (Lu et al., 1995). Meanwhile, the contemporaneous garnet-bearing quartz monzonite (2134 ± 17 Ma) and slightly older potassic granites in the Lushan area (2194 ± 29 Ma) show intermediate shoshonitic and fractionated aluminous A-type granites in compositions, respectively. Both of them were formed in extensional or intra-continental rift settings (Zhou et al., 2014, 2015). The coeval metamorphosed mafic dykes (2128 ± 29 Ma) recognized in the Lushan area were also suggested to have emplaced in rift-related, or more precisely in an extensional setting (Sun et al., 2017b).

On the other hand, the late Paleoproterozoic sequence-set in the southern NCC comprises the 1.91–1.80 Ga Tietonggou Formation in the Xiaoqinling area and the 1.85–1.78 Ga Danshanshi Group in the Zhongtiaoshan area, both of which consists mainly of metaconglomerates and meta-sandstones, whose depositional setting were estimated in a retro-arc foreland basin (Liu et al., 2012b; Diwu et al., 2013), similar with the Fangniushan supracrustal strata in the Xiaoshan area. Therefore, we suggest that the Fangniushan rock associations were formed during closure of the pre-existing extension-related basin in the final cratonization of the NCC.

Taken together, we prefer that the southern NCC might have experienced a tectonic change from rift to subduction during Paleoproterozoic. Nevertheless, the mechanism of rift evolution and the time of subduction initiation are still unresolved and need to be further studied in the future.

6. Conclusions

Based on the detailed zircon U-Pb and Lu-Hf isotope compositions, and whole-rock geochemical data, we can draw the following main conclusions:

- (1) The Fangniushan supracrustal strata in the Xiaoshan area was deposited at ca. 1.87–1.80 Ga.
- (2) The Fangniushan metasedimentary rocks dominantly received detritus from felsic sources in the Xiaoshan and adjacent Xiaoqinling, Xiongershan and Zhongtiaoshan areas.
- (3) The Fangniushan supracrustal strata was most likely formed in a retro-arc foreland setting, while the southern NCC might have experienced tectonic regime change from rift to subduction during Paleoproterozoic.

Declaration of Competing Interest

The authors declare that they have no known competing financial interests or personal relationships that could have appeared to influence the work reported in this paper.

Acknowledgements

This study was financially supported by the National Natural Science Foundation of China (No. 41802203 and No. 41573041). We are grateful to the assistance of Dr. Dan Wu, Qiang Wu and engineer Le Zhang during zircon U-Pb dating and Lu-Hf analyses. Engineer Xianglin Tu and Dr. Xinyu Wang are thanked for their assistance during ICP-MS

and XRF analyses. Two anonymous reviewers and guest editor Prof. Jian Zhang are greatly thanked for their constructive comments on this paper. This is contribution No. IS-2865 from GIGCAS.

References

- Andersen, T., 2005. Detrital zircons as tracers of sedimentary provenance: limiting conditions from statistics and numerical simulation. *Chem. Geol.* 216, 249–270.
- Bekker, A., Holland, H.D., Wang, P.L., Rumble III, D., Stein, H.J., Hannah, J.L., Coetzee, L.L., Beukes, N.J., 2004. Dating the rise of atmospheric oxygen. *Nature* 427, 117–120.
- Bhatia, M.R., 1983. Plate tectonics and geochemical composition of sandstones. *J. Geol.* 91, 611–627.
- Bhatia, M.R., Crook, K.A.W., 1986. Trace element characteristics of graywackes and tectonic setting discrimination of sedimentary basins. *Contrib. Miner. Petrol.* 92, 181–193.
- Bureau of Geology and Mineral Resources of Henan Province, 1995. 1:50000 regional geological survey report of Xiaoshan region (in Chinese).
- Bouvier, A., Vervoort, J.D., Patchett, P.J., 2008. The Lu-Hf and Sm-Nd isotopic composition of chur: constraints from unequilibrated Chondrites and implications for the bulk composition of terrestrial planets. *Earth Planet. Sci. Lett.* 273, 48–57.
- Chen, H.X., Wang, H.Y.C., Peng, T., Wu, C.M., 2016. Petrogenesis and geochronology of the Neoarchean-Paleoproterozoic granitoid and monzonitic gneisses in the Taihua complex: episodic magmatism of the southwestern Trans-North China Orogen. *Precambr. Res.* 287, 31–47.
- Chen, H.X., Liu, J.H., Zhang, Q.W.L., Wang, H.Y.C., Wu, C.M., 2020. A long-lived tectono-metamorphic event in the late Paleoproterozoic: evidence from SIMS U-Th-Pb dating of monazite from metapelite in central-south Trans-North China Orogen. *Precambr. Res.* 336, 105497.
- Cawood, P.A., Hawkesworth, C.J., Dhuime, B., 2012. Detrital zircon record and tectonic setting. *Geology* 40, 875–878.
- Condie, K.C., 1993. Chemical composition and evolution of the upper continental crust: contrasting results from surface samples and shales. *Chem. Geol.* 104, 1–37.
- Condie, K.C., 1997. Plate Tectonics and Crustal Evolution. Butterworth-Heinemann, Oxford, pp. 1–281.
- Cox, R., Lowe, D.R., Cullers, R.L., 1995. The influence of sediment recycling and basement composition on evolution of mudrock chemistry in the southwestern United States. *Geochim. Cosmochim. Acta* 59 (14), 2919–2940.
- Chu, N.C., Taylor, R.N., Chavagnac, V., Nesbitt, R.W., Boella, R.M., Milton, J.A., German, C.R., Bayon, G., Burton, K., 2002. Hf isotope ratio analysis using multi-collector inductively coupled plasma mass spectrometry: an evaluation of isobaric interference corrections. *J. Anal. At. Spectrom.* 17 (12), 1567–1574.
- Cullers, R.L., 2000. The geochemistry of shales, siltstones, and sandstones of Pennsylvanian-Permian age, Colorado, USA: implications for provenance and metamorphic studies. *Lithos* 51, 181–203.
- Cullers, R.L., Podkorytov, V.N., 2000. Geochemistry of the Mesoproterozoic Lakhanda shales in southeastern Yakutia, Russia: implications for mineralogical and provenance control, and recycling. *Precambr. Res.* 104, 77–93.
- DeCelles, P.G., Giles, K.A., 1996. Foreland basin systems. *Basin Res.* 8, 105–123.
- DeGraaff-Surpless, K., Graham, S.A., Wooden, J.L., McWilliams, M.O., 2002. Detrital zircon provenance analysis of the Great Valley Group, California: evolution of an arc-forearc system. *Geol. Soc. Am. Bull.* 114, 1564–1580.
- Deng, X.Q., Peng, T.P., Zhao, T.P., 2016. Geochronology and geochemistry of the late Paleoproterozoic aluminous A-type granite in the Xiaoqinling area along the southern margin of the North China Craton: petrogenesis and tectonic implications. *Precambr. Res.* 285, 127–146.
- Diwu, C.R., Sun, Y., Lin, C.L., Li, H.P., Chen, L., Liu, X.M., 2007. Formation history of Archaean TTG gneisses in the Taihua complex, Lushan area, central China: in situ U-Pb age and Hf-isotope analysis of zircons. *Geochim. Cosmochim. Acta* 71 (15), A226.
- Diwu, C.R., Sun, Y., Yuan, H.L., Wang, H.L., Zhong, X.P., Liu, X.M., 2008. U-Pb ages and Hf isotopes for detrital zircons from quartzite in the Paleoproterozoic Songshan Group on the southwestern margin of the North China Craton. *Chin. Sci. Bull.* 53 (18), 2828–2839.
- Diwu, C.R., Sun, Y., Lin, C.L., Wang, H.L., 2010. LA-(MC)-ICPMS U-Pb zircon geochronology and Lu-Hf isotope compositions of the Taihua complex on the southern margin of the North China Craton. *Chin. Sci. Bull.* 55, 2557–2571.
- Diwu, C.R., Sun, Y., Gao, J.F., Fan, L.G., 2013. Early Precambrian tectonothermal events of the North China Craton: Constraints from in situ detrital zircon U-Pb, Hf and O isotopic compositions in Tietonggou Formation. *Chin. Sci. Bull.* 58, 3760–3770.
- Diwu, C.R., Sun, Y., Zhao, Y., Lai, S.C., 2014. Early Paleoproterozoic (2.45–2.20 Ga) magmatic activity during the period of global magmatic shutdown: Implications for the crustal evolution of the southern North China Craton. *Precambr. Res.* 255, 627–640.
- Diwu, C.R., Liu, X., Sun, Y., 2018. The composition and evolution of the Taihua Complex in the southern North China Craton. *Acta Petrol. Sin.* 34 (4), 999–1018 (in Chinese with English abstract).
- Du, L.L., Yang, C.H., Ren, L.D., Wan, Y.S., Wu, J.S., 2009. Petrology, geochemistry and petrogenesis of the metabasalts of the Hutuo Group, Wutai Mountains, Shanxi, China. *Geol. Bull. China* 28, 867–876 (in Chinese with English abstract).
- Du, L.L., Yang, C.H., Guo, J.H., Wang, W., Ren, L.D., Wan, Y.S., Geng, Y.S., 2010. The age of the base of the Paleoproterozoic Hutuo Group in the Wutai Mountains area, North China Craton: SHRIMP zircon U-Pb dating of basaltic andesite. *Chin. Sci. Bull.* 55, 1782–1789.
- Du, L.L., Yang, C.H., Wyman, D.A., Nutman, A.P., Zhao, L., Lu, Z.L., Song, H.X., Geng, Y.S., Ren, L.D., 2017. Zircon U-Pb ages and Lu-Hf isotope compositions from clastic

- rocks in the Hutuo Group: further constraints on Paleoproterozoic tectonic evolution of the Trans-North China Orogen. *Precambr. Res.* 303, 291–314.
- Faure, M., Trap, P., Lin, W., Monie, P., Bruguier, O., 2007. Polyorogenic evolution of the Paleoproterozoic Trans-North China Belt: new insights from the Luliangshan-Hengshan-Wutaishan and Fuping massifs. *Episodes* 30, 95–106.
- Fedo, C.M., Nesbitt, H.W., Young, G.M., 1995. Unraveling the effects of potassium metasomatism in sedimentary rocks and paleosols, with implications for paleo-weathering conditions and provenance. *Geology* 23, 921–924.
- Fedo, C.M., Sircombe, K.N., Rainbird, R.H., 2003. Detrital zircon analysis of the sedimentary record, Zircon. In: Hanchar, J.M., Hoskin, P.W.O. (Eds.), *Rev. Mineral. Geochem.* J. 53, pp. 277–303.
- Floyd, P., Leveridge, B., 1987. Tectonic environment of the Devonian Gramscatho basin, south Cornwall: framework mode and geochemical evidence from turbiditic sandstones. *J. Geol. Soc.* 144, 531–540.
- Gehrels, G.E., Valencia, V., Pullen, A., 2006. Detrital zircon geochronology by laser-ablation multicollector ICPMS at the Arizona Laser-Chron Center. In: Olszewski, T., Huff, W. (Eds.), *Geochronology: Emerging opportunities*: Philadelphia. Paleontological Society Short Course, Pennsylvania, pp. 1–10.
- Geng, Y.S., Wan, Y.S., Yang, C.H., 2003. The Paleoproterozoic rift-type volcanism in Luliangshan area, Shanxi Province, and its geological significance. *Acta Petrol. Sin.* 24, 97–104 (in Chinese with English abstract).
- Geng, Y.S., Wan, Y.S., Yang, C.H., 2008. Integrated research report on the establishment of Paleoproterozoic system of China: Determination of major Paleoproterozoic geological events and preliminary subdivision of Paleoproterozoic strata in the Luliang area. Research Report on the Establishment of Major Stratigraphical Stages in China (2001–2005). Geological Publishing House, Beijing, pp. 515–533.
- Griffin, W.L., Pearson, N.J., Belousova, E., Jackson, S.E., van Achterbergh, E., O'Reilly, S.Y., Shee, S.R., 2000. The Hf isotope composition of cratonic mantle: LAM-MC-ICPMS analysis of zircon megacrysts in kimberlites. *Geochim. Cosmochim. Acta* 64 (1), 133–147.
- Griffin, W.L., Wang, X., Jackson, S.E., Pearson, S.E., O'Reilly, S.Y., Xu, X.S., Zhou, X.M., 2002. Zircon chemistry and magma genesis, SE China: in-situ analysis of Hf isotopes, Tonglu and Pingtan Igneous complexes. *Lithos* 61, 237–269.
- Guo, L.S., Liu, S.W., Liu, Y.L., Tian, W., Yu, S.Q., Li, Q.G., Lü, Y.J., 2008. Zircon Hf isotopic features of TTG gneissed and formation environment of Precambrian Sushui Complex in Zhongtiao mountains. *Acta Petrol. Sin.* 24, 139–148 (in Chinese with English abstract).
- He, Y.H., Zhao, G.C., Sun, M., Xia, X.P., 2009. SHRIMP and LA-ICP-MS zircon geochronology of the Xiong'er volcanic rocks: implications for the Paleo-Mesoproterozoic evolution of the southern margin of the North China Craton. *Precambr. Res.* 168, 213–222.
- Herron, M.M., 1988. Geochemical classification of terrigenous sands and shales from core or log data. *J. Sediment. Petrol.* 58, 820–829.
- Hofmann, A., 2005. The geochemistry of sedimentary rocks from the Fig Tree Group, Barberton greenstone belt: implications for tectonic, hydrothermal and surface processes during Mid-Archaean times. *Precambr. Res.* 143 (1–4), 23–49.
- Holland, H.D., 2002. Volcanic gases, black smokers, and the Great Oxidation Event. *Geochim. Cosmochimica Acta* 66, 3811–3826.
- Hoskin, P.W.O., Black, L.P., 2000. Metamorphic zircon formation by solid-state recrystallization of protolith igneous zircon. *J. Metamorph. Geol.* 18, 423–439.
- Hou, G.T., Santosh, M., Qian, X.L., Lister, G.S., Li, J.H., 2008. Configuration of the Late Paleoproterozoic supercontinent Columbia: insights from radiating mafic dyke swarms. *Gondwana Res.* 14, 395–409.
- Huang, X.L., Wilde, S.A., Yang, Q.J., Zhong, J.W., 2012. Geochronology and petrogenesis of gray gneisses from the Taihua Complex at Xiong'er in the southern segment of the Trans-North China Orogen: implications for tectonic transformation in the Early Paleoproterozoic. *Lithos* 134–135, 236–252.
- Huang, X.L., Wilde, S.A., Zhong, J.W., 2013. Episodic crustal growth in the southern segment of the Trans-North China Orogen across the Archean-Proterozoic boundary. *Precambr. Res.* 233, 337–357.
- Jia, X.L., Zhu, X.Y., Zhai, M.G., Zhao, Y., Zhang, H., Wu, J.L., Liu, T., 2016. Late Mesoarchean crust growth event: evidence from the ca. 2.8 Ga granodioritic gneisses of the Xiaojinling area, southern North China Craton. *Chin. Sci. Bull.* 61 (12), 974–990.
- Jia, X.L., Zhai, M.G., Xiao, W.J., Li, L., Ratheesh-Kumar, R.T., Wu, J.L., Liu, Y., 2020. Mesoarchean to Paleoproterozoic crustal evolution of the Taihua Complex in the southern North China Craton. *Precambr. Res.* 337, 105451.
- Kröner, A., Wilde, S.A., Li, J.H., 2005. Age and evolution of a late Archean to Paleoproterozoic upper to lower crustal section in the Wutaishan/Hengshan/Fuping terrain of northern China. *J. Asian Earth Sci.* 24, 577–595.
- Kusky, T.M., Li, J.H., Tucker, R.D., 2001. The Archean Dongwanzi ophiolite complex, North China Craton: 2.505 billion year old oceanic crust and mantle. *Science* 292, 1142–1145.
- Kusky, T.M., Li, J.H., 2003. Paleoproterozoic tectonic evolution of the North China Craton. *J. Asian Earth Sci.* 22, 383–397.
- Kusky, T.M., 2011. Geophysical and geological tests of tectonic models of the North China Craton. *Gondwana Res.* 20, 26–35.
- Kusky, T.M., Zhai, M.G., 2012. The Neoproterozoic ophiolite in the North China Craton: early Precambrian plate tectonics and scientific debate. *J. Earth Sci.* 23, 277–284.
- Li, J.H., Kusky, T.M., Huang, X., 2002. Neoarchean podiform chromites and harzburgite tectonite in ophiolitic mélange, North China Craton, remnants of Archean oceanic mantle. *GSA Today* 12, 4–11.
- Li, C.Y., Zhang, R.Q., Ding, X., Ling, M.X., Fan, W.M., Sun, W.D., 2015. Dating cassiterite using laser ablation ICP-MS. *Ore Geol. Rev.* 72, 313–322.
- Li, S.Z., Zhao, G.C., Wilde, S.A., Zhang, J., Sun, M., Zhang, G.W., Dai, L.M., 2010a. Deformation history of the Hengshan-Wutai-Fuping complexes: implications for the evolution of the Trans-North China Orogen. *Gondwana Res.* 18, 611–631.
- Li, S.Z., Zhao, G.C., Santos, M., Liu, X., Dai, L.M., Suo, Y.H., Tam, P.Y., Song, M.C., Wang, P.C., 2012. Paleoproterozoic structural evolution of the southern segment of the Jiao-Liao-Ji Belt, North China Craton. *Precambr. Res.* 200, 59–73.
- Li, X.H., 1997. Geochemistry of the Longsheng Ophiolite from the southern margin of Yangtze Craton, SE China. *Geochem. J.* 31 (5), 323–337.
- Li, X.H., Li, Z.X., Wingate, M.T.D., Chung, S.L., Liu, T., Lin, G.C., Li, W.X., 2006. Geochemistry of the 755 Ma Mundine Well dyke swarm, northwestern Australia: part of a Neoproterozoic mantle superplume beneath Rodinia? *Precambr. Res.* 146, 1–15.
- Li, X.H., Long, W.G., Li, Q.L., Liu, Y., Zheng, Y.F., Yang, Y.H., Chamberlain, K.R., Wan, D.F., Guo, C.H., Wang, X.C., Tao, H., 2010b. Penglai zircon megacrysts: a potential new working reference material for microbeam determination of Hf-O isotopes and U-Pb age. *Geostand. Geoanal. Res.* 34, 117–134.
- Liu, C.H., Zhao, G.C., Sun, M., Zhang, J., He, Y.H., Yin, C.Q., Wu, F.Y., Yang, J.H., 2011. U-Pb and Hf isotopic study of detrital zircons from the Hutuo group in the Trans-North China Orogen and tectonic implications. *Gondwana Res.* 20, 106–121.
- Liu, C.H., Zhao, G.C., Sun, M., Zhang, J., Yin, C.Q., 2012a. Detrital zircon U-Pb dating, Hf isotopes and whole-rock geochemistry from the Songshan Group in the Dengfeng Complex: constraints on the tectonic evolution of the Trans-North China Orogen. *Precambr. Res.* 192–195, 1–15.
- Liu, C.H., Zhao, G.C., Sun, M., Zhang, J., Yin, C.Q., 2012b. U-Pb geochronology and Hf isotope geochemistry of detrital zircons from the Zhongtiao Complex: constraints on the tectonic evolution of the Trans-North China Orogen. *Precambr. Res.* 222–223, 159–172.
- Liu, C.H., Zhao, G.C., Liu, F.L., Shi, J.R., Ji, L., Liu, P.H., Yang, H., Liu, L.S., Wang, W., Tian, Z.H., 2016. Zircon U-Pb and Lu-Hf isotopic and whole-rock geochemical constraints on the Lanhe and Heichashan Groups: implications for the Paleoproterozoic tectonic basin evolution of the Luliang Complex. *Lithos* 262, 526–545.
- Liu, C.H., Zhao, G.C., Liu, F.L., Shi, J.R., 2017. Detrital zircon U-Pb and Hf isotopic and whole-rock geochemical study of the Bayan Obo Group, northern margin of the North China Craton: implications for Rodinia reconstruction. *Precambr. Res.* 303, 372–391.
- Liu, C.H., Zhao, G.C., Liu, F.L., Cai, J., 2018. The southwestern extension of the Jiao-Liao-Ji belt in the North China Craton: geochronological and geochemical evidence from the Wuhe Group in the Bengbu area. *Lithos* 304–307, 258–279.
- Liu, D.Y., Nutman, A.P., Compston, W., Wu, J.S., Shen, Q.H., 1992. Remnants of ≥ 3800 Ma crust in the Chinese part of the Sino-Korean Craton. *Geology* 20, 339–342.
- Liu, D.Y., Wilde, S.A., Wan, Y.S., Wu, J.S., Zhou, H.Y., Dong, C.Y., Yin, X.Y., 2008. New U-Pb and Hf isotopic data confirm Anshan as the oldest preserved segment of the North China Craton. *Am. J. Sci.* 308, 200–231.
- Liu, Y.S., Hu, Z.C., Zong, K.Q., Gao, C.G., Gao, S., Xu, J., Chen, H.H., 2010. Reappraisement and refinement of zircon U-Pb isotope and trace element analyses by LA-ICP-MS. *Chin. Sci. Bull.* 55, 1535–1546.
- Lu, Z., Xu, X., Liu, F., 1995. The Precambrian Khondalite Series in the North of China. Changchun Publishing House, Changchun, pp. 245–251.
- Lu, J.S., Wang, G.D., Wang, H., Chen, H.X., Wu, C.M., 2013. Metamorphic P-T-t paths retrieved from the amphibolites, Lushan terrane, Henan Province and reappraisal of the Paleoproterozoic tectonic evolution of the Trans-North China Orogen. *Precambr. Res.* 238, 61–77.
- Lu, J.S., Wang, G.D., Wang, H., Chen, H.X., Wu, C.M., 2014. Palaeoproterozoic metamorphic evolution and geochronology of the Wugang block, southeastern terminal of the Trans-North China Orogen. *Precambr. Res.* 251, 197–211.
- Lu, J.S., Zhai, M.G., Long, X.P., 2020. Paleoproterozoic tectono-metamorphic evolution of the southernmost North China Craton: new insights from the metamorphic evolution and geochronology of the Taihua complex at Lushan area. *Precambr. Res.* 342, 105693.
- Ludwig, K.R., 2003. User's Manual for ISOPLOT 3.00: A Geochronological Toolkit for Microsoft Excel, Special Publication No. 4. Berkeley Geochronology Center, pp. 71.
- Luo, Z.X., 2016. Geochronology, geochemistry and petrogenesis of the Xiaoshan Taihua Complex in the southern segment of the Trans-North China Orogen. (Master thesis). University of Chinese Academy of Sciences, China.
- Luo, Z.X., Huang, X.L., Wang, X., Yang, F., Han, L., 2018. Geochronology and Geochemistry of the TTG Gneisses from the Taihua Group in the Xiaoshan Area, North China Craton: Constraints on Petrogenesis. *Geotectonica et Metallogenesis* 42 (2), 332–347 (in Chinese with English abstract).
- Lyons, T.W., Reinhard, C.T., Planavsky, N.J., 2014. The rise of oxygen in Earth's early ocean and atmosphere. *Nature* 506, 307–314.
- Machado, N., Siminetti, A., 2001. U-Pb dating and Hf isotopic composition of zircon by laser-ablation MC-ICP-MS. In: Sylvester, P. (Ed.), *Laser Ablation-ICPMS in the Earth Sciences: Principles and Applications*. St. John's, Newfoundland, Mineralogical Association of Canada, pp. 121–146.
- McLennan, S.M., Taylor, S.R., 1991. Sedimentary rocks and crustal evolution: tectonic setting and secular trends. *J. Geol.* 99, 1–21.
- McLennan, S.M., Hemming, S., McDaniel, D.K., Hannson, G.N., 1993. Geochemical approaches to sedimentation, provenance and tectonics. *Geol. Soc. Am. Special Papers* 284, 21–40.
- Nesbitt, H.W., Young, G.M., 1982. Early Proterozoic climates and plate motions inferred from major element chemistry of lutites. *Nature* 299, 715–717.
- Nesbitt, H.W., Young, G.M., 1984. Prediction of some weathering trends of plutonic and volcanic rocks based on thermodynamic and kinetic considerations. *Geochim. Cosmochim. Acta* 48, 1423–1534.
- Nesbitt, H.W., Young, G.M., 1989. Formation and diagenesis of weathering profiles. *J. Geol.* 97, 129–147.
- Peng, P., Zhai, M.G., Ernst, R.E., Guo, J.H., Liu, F., Hu, B., 2008. A 1.78 Ga large igneous province in the North China Craton: The Xiong'er volcanic province and the North China dyke swarm. *Lithos* 101 (3–4), 260–280.
- Polat, A., Li, J.H., Fryer, B., Kusky, T., Kerrich, R., Gagnon, J., Zhang, S., 2006.

- Geochemical characteristics of the Neoarchean (2800–2700 Ma) Taishan greenstone belt, North China Craton: evidence for plume–craton interaction. *Chem. Geol.* 230, 60–87.
- Roddaz, M., Viers, J., Brusset, S., Baby, P., Boucayrand, C., Héral, G., 2006. Controls on weathering and provenance in the amazonian foreland basin: insights from major and trace element geochemistry of neogene amazonian sediments. *Chem. Geol.* 226, 31–65.
- Roser, B.P., Korsch, R.J., 1986. Determination of tectonic setting of sandstone–mudstone suites using SiO_2 content and $\text{K}_2\text{O}/\text{Na}_2\text{O}$ ratio. *J. Geol.* 94 (5), 635–650.
- Rudnick, R.L., Gao, S., 2003. Composition of the continental crust. *Treatise Geochemistry* 3, 1–64.
- Slack, J.F., Stevens, P.J., 1994. Clastic metasediments of the Early Proterozoic Broken Hill Group, New South Wales, Australia: geochemistry, provenance and metallogenetic significance. *Geochim. Cosmochim. Acta* 58, 3633–3652.
- Sugitani, K., Yamashita, F., Nagaoka, T., Yamamoto, K., Minamie, M., Mimurad, K., Suzuki, K., 2006. Geochemistry and sedimentary petrology of Archean clastic sedimentary rocks at Mt. Goldsworthy, Pilbara Craton, Western Australia: evidence for the early evolution of continental crust and hydrothermal alteration. *Precambr. Res.* 147 (1–2), 124–147.
- Sun, D.Z., Li, H.M., Lin, Y.X., et al., 1991. Precambrian geochronology, chronotectonic framework and model of chronocrustal structure of the Zhongtiao Mountains. *Acta Geol. Sin.* 3, 216–231 (in Chinese with English abstract).
- Sun, D.Z., Hu, W.X., 1993. The Geochronological Framework and Crustal Structures of Precambrian Basement in the Zhongtiaoshan Area 108–117 (in Chinese).
- Sun, Q.Y., Zhou, Y.Y., Zhao, T.P., Wang, W., 2017a. Geochronology and geochemistry of the Paleoproterozoic Yinyougou Group in the southern North China Craton: implications for provenance and tectonic evolution. *Precambr. Res.* 296, 120–147.
- Sun, Q.Y., Zhou, Y.Y., Wang, W., Li, C.D., Zhao, T.P., 2017b. Formation and evolution of the Paleoproterozoic meta-mafic and associated supracrustal rocks from the Lushan Taihua Complex, southern North China Craton: insights from zircon U-Pb geochronology and whole-rock geochemistry. *Precambr. Res.* 303, 428–444.
- Sun, S.S., McDonough, W.F., 1989. Chemical and isotopic systematic of oceanic basalts: implications for mantle composition and process. In: Saunders, A.D., Norry, M.J. (Eds.), *Magma in the Ocean Basins: Geological Society Special Publication* 42, pp. 313–345.
- Sun, Y., 1983. Rocks in the granulite facies of the Taihua Group at Lushan. *Henan. J. Northwest Univ.* 38, 89–95 (in Chinese with English abstract).
- Taylor, S.R., McLennan, S.M., 1985. *The Continental Crust: Its Composition and Evolution*. Blackwell Scientific Publications, Oxford, UK, pp. 312.
- Tian, W., Liu, S.W., Liu, C.H., Yu, S.Q., Li, Q.G., Wang, Y.R., 2006. Zircon SHRIMP geochronology and geochemistry of TTG rocks in Sushui Complex from Zhongtiao Mountains with its geological implications. *Prog. Nat. Sci.* 16, 492–500.
- Trap, P., Faure, M., Lin, W., Monié, P., 2007. Late Paleoproterozoic (1900–1800 Ma) nappe stacking and polyphase deformation in the Hengshan-Wutaishan area: implications for the understanding of the Trans-North-China Belt, North China Craton. *Precambr. Res.* 156, 85–106.
- Trap, P., Faure, M., Lin, W., Bruguier, O., Monié, P., 2008. Contrasted tectonic styles for the Paleoproterozoic evolution of the North China Craton. Evidence for a 2.1 Ga thermal and tectonic event in the Fuping Massif. *J. Struct. Geol.* 30, 1109–1125.
- Trap, P., Faure, M., Lin, W., Augier, R., Fouassier, A., 2011. Syn-collisional channel flow and exhumation of Paleoproterozoic high pressure rocks in the Trans North China Orogen: the critical role of partial-melting and orogenic bending. *Gondwana Res.* 20, 498–515.
- Trap, P., Faure, M., Lin, W., et al., 2012. Paleoproterozoic tectonic evolution of the Trans-North China Orogen: toward a comprehensive model. *Precambr. Res.* 222–223, 191–211.
- Van de Kamp, P.C., Leake, B.E., 1985. Petrography and geochemistry of feldspathic and mafic sediments of the northeastern Pacific margin. *Trans. R. Soc. Edinb. Earth Sci.* 76, 411–499.
- Vavra, G., Schmid, R., Gebauer, D., 1999. Internal morphology, habit and U-Th-Pb microanalysis of amphibole to granulite facies zircon: geochronology of the Ivren Zone (Southern Alps). *Contrib. Miner. Petrol.* 134, 380–404.
- Wan, Y.S., Wilde, S.A., Liu, D.Y., Yang, C.X., Song, B., Yin, X.Y., 2006. Further evidence for 1.85 Ga metamorphism in the Central Zone of the North China Craton: SHRIMP U-Pb dating of zircon from metamorphic rocks in the Lushan area, Henan Province. *Gondwana Res.* 9, 189–197.
- Wan, Y.S., Liu, D.Y., Wang, S.Y., Zhao, X., Dong, C.Y., Zhou, H.Y., Yin, X.Y., Yang, C.X., Gao, L.Z., 2009. Early Precambrian crustal evolution in the Dengfeng Area, Henan Province (eastern China): constraints from geochemistry and SHRIMP U-Pb zircon dating. *Acta Geol. Sin.* 83, 982–999 (in Chinese with English abstract).
- Wan, Y.S., Xu, Z.Y., Dong, C.Y., Nutman, A., Ma, M.Z., Xie, H.Q., Liu, S., Liu, D.Y., Wang, H., Cu, H., 2013. Episodic Paleoproterozoic (~2.45, ~1.95 and ~1.85 Ga) mafic magmatism and associated high temperature metamorphism in the Daqingshan area, North China Craton: SHRIMP zircon U-Pb dating and whole-rock geochemistry. *Precambr. Res.* 224, 71–93.
- Wang, G.D., Wang, H., Chen, H.X., Zhang, B., Zhang, Q., Wu, C.M., 2017a. Geochronology and geochemistry of the TTG and potassic granite of the Taihua Complex, Mts. Huashan: implications for crustal evolution of the southern North China Craton. *Precambr. Res.* 288, 72–90.
- Wang, W., Chen, F.K., Hu, R., Chu, Y., Yang, Y.Z., 2012. Provenance and tectonic setting of Neoproterozoic sedimentary sequences in the South China Block: evidence from detrital zircon ages and Hf-Nd isotopes. *Int. J. Earth Sci.* 101, 1723–1744.
- Wang, W., Zhou, M.F., 2013. Petrological and geochemical constraints on provenance, paleoweathering and tectonic setting of the Neoproterozoic sedimentary basin in the eastern Jiangnan Orogen, South China. *J. Sediment. Res.* 83, 974–993.
- Wang, W., Cawood, P.A., Zhou, M.F., Pandit, M.K., Chen, W.T., 2017b. Zircon U-Pb age and Hf isotope evidence for Eoarchean crustal remnant, and crustal growth and reworking respond to supercontinental cycles in NW India. *J. Geol. Soc. Jgs* 2016–2080.
- Wang, W., Zeng, M.F., Zhou, M.F., Zhao, J.H., Zheng, J.P., Lan, Z.F., 2018a. Age, provenance and tectonic setting of Neoproterozoic to early Paleozoic sequences in southeastern South China Block: constraints on its linkage to western Australia-East Antarctica. *Precambr. Res.* 309, 290–308.
- Wang, W., Zhao, J.H., Zhou, M.F., Pandit, M.K., Zheng, J.P., 2018b. Depositional age, provenance characteristics and tectonic setting of the meso-and Neoproterozoic sequences in SE Yangtze Block, China: implications on Proterozoic supercontinent reconstructions. *Precambr. Res.* 309, 231–347.
- Wang, X.L., Jiang, S.Y., Dai, B.Z., 2010. Melting of enriched Archean subcontinental lithospheric mantle: evidence from the ca. 1760 Ma volcanic rocks of the Xiong'er Group, southern margin of the North China Craton. *Precambr. Res.* 182, 204–216.
- Wilde, S.A., Zhao, G.C., Sun, M., 2002. Development of the North China Craton during the Late Archaean and its final amalgamation at 1.8 Ga; some speculations on its position within a global Palaeoproterozoic Supercontinent. *Gondwana Res.* 5, 85–94.
- Wu, F.Y., Yang, Y.H., Xie, L.W., Yang, J.H., Xu, P., 2006. Hf isotopic compositions of the standard zircons and baddeleyites used in U-Pb geochronology. *Chem. Geol.* 234, 105–126.
- Wu, F.Y., Zhang, Y.B., Yang, J.H., Xie, L.W., Yang, Y.H., 2008. Zircon U-Pb and Hf isotopic constraints on the Early Archean crustal evolution in Anshan of the North China Craton. *Precambr. Res.* 167, 339–362.
- Xu, P., Wu, F.Y., Xie, L.W., Yang, Y.H., 2004. Hf isotopic compositions of the standard zircons for U-Pb dating. *Chin. Sci. Bull.* 49, 1642–1648.
- Yu, S.Q., Liu, S.W., Tian, W., Li, Q.G., Feng, Y.G., 2006. SHRIMP Zircon U-Pb Chronology and Geochemistry of the Henglingguan and Beiyu Granitoids in the Zhongtiao Mountains, Shanxi Province. *Acta Geol. Sin.* 80, 912–924 (in Chinese with English abstract).
- Yu, X.Q., Liu, J.L., Li, C.L., Chen, S.Q., Dai, Y.P., 2013. Zircon U Pb dating and Hf isotope analysis on the Taihua Complex: constraints on the formation and evolution of the Trans North China Orogen. *Precambr. Res.* 230, 31–44.
- Zhai, M.G., Bian, A.G., Zhao, T.P., 2000. The amalgamation of the supercontinent of North China Craton at the end of Neo-Archaean and its breakup during late Palaeoproterozoic and Meso-Proterozoic. *Sci. China (series D)* 43 (1), 219–232.
- Zhai, M.G., Guo, J.H., Liu, W.J., 2005. Neoarchean continental evolution and tectonic history of the North China Craton: a review. *J. Asian Earth Sci.* 24, 547–561.
- Zhai, M.G., Santosh, M., 2011. The early Precambrian odyssey of the North China Craton: a synoptic overview. *Gondwana Res.* 20, 6–25.
- Zhai, M.G., Santosh, M., 2013. Metallogeny of the North China Craton: link with secular changes in the evolving Earth. *Gondwana Res.* 24, 275–297.
- Zhai, M.G., 2014. Multi-stage crustal growth and cratonization of the North China Craton. *Geosci. Front.* 5 (4), 457–469.
- Zhang, R.Y., Zhang, C.L., Diwu, C.R., Sun, Y., 2012. Zircon U-Pb geochronology, geochemistry and its geological implications for the Precambrian granitoids in Zhongtiao Mountain, Shanxi Province. *Acta Petrol. Sin.* 28 (11), 3559–3573 (in Chinese with English abstract).
- Zhang, R.Y., Zhang, C.L., Diwu, C.R., Sun, Y., 2013. Crustal reworking in the North China Craton at ~2.5 Ga: evidence from zircon U-Pb ages, Hf isotopes and whole-rock geochemistry of the TTG gneisses in the Zhongtiao Mountain. *Acta Petrol. Sin.* 29 (7), 2265–2280 (in Chinese with English abstract).
- Zhao, B., Wang, D.H., Hou, K.J., Liu, R.J., 2012a. Isochronology study on Sushui Complex in Zhongtiao Mountains and its geological significance. *J. Earth Sci. Environ.* 34 (1), 1–8 (in Chinese with English abstract).
- Zhao, G.C., Cawood, P.A., Wilde, S.A., Sun, M., Lu, L.Z., 2000. Metamorphism of basement rocks in the Central Zone of the North China Craton: Implications for Paleoproterozoic tectonic evolution. *Precambr. Res.* 103 (1–2), 55–88.
- Zhao, G.C., Wilde, S.A., Cawood, P.A., Sun, M., 2001. Archean blocks and their boundaries in the North China Craton: lithological, geochemical, structural and P-T path constraints and tectonic evolution. *Precambr. Res.* 107 (1–2), 45–73.
- Zhao, G.C., Sun, M., Wilde, S.A., Li, S.Z., 2004a. A Paleo-Mesoproterozoic supercontinent: assembly, growth and breakup. *Earth Sci. Rev.* 67, 91–123.
- Zhao, G.C., Sun, M., Wilde, S.A., Li, S.Z., 2005. Late Archean to Paleoproterozoic evolution of the North China Craton: key issues revisited. *Precambr. Res.* 136, 177–202.
- Zhao, G.C., Wilde, S.A., Sun, M., Guo, J.H., Kröner, A., Li, S.Z., Li, X.P., Zhang, J., 2008. Shrimp U-Pb zircon geochronology of the Huai'an Complex: Constraints on Late Archean to paleoproterozoic magmatic and metamorphic events in the Trans-North China Orogen. *Am. J. Sci.* 308, 270–303.
- Zhao, G.C., He, Y.H., Sun, M., 2009. The Xiong'er volcanic belt at the southern margin of the North China Craton: petrographic and geochemical evidence for its outboard position in the Paleo-mesoproterozoic Columbia Supercontinent. *Gondwana Res.* 16 (2), 170–181.
- Zhao, G.C., Li, S.Z., Sun, M., Wilde, S.A., 2011. Assembly, accretion, and break-up of the Paleo-Mesoproterozoic Columbia supercontinent: record in the North China Craton revisited. *Int. Geol. Rev.* 53, 1331–1356.
- Zhao, G.C., Cawood, P.A., Li, S.Z., Wilde, S.A., Sun, M., Zhang, J., He, Y.H., Yin, C.Q., 2012b. Amalgamation of the North China Craton: key issues and discussion. *Precambr. Res.* 222–223, 55–76.
- Zhao, T.P., Zhou, M.F., Zhai, M.G., Xia, B., 2002. Paleoproterozoic rift-related volcanism of the Xiong'er Group, North China craton: implications for the breakup of Columbia. *Int. Geol. Rev.* 44, 336–351.
- Zhao, T.P., Zhai, M.G., Xia, B., Li, H.M., Zhang, Y.X., Wan, Y.S., 2004b. Zircon U-Pb SHRIMP dating for the volcanic rocks of the Xiong'er Group: constraints on the initial formation age of the cover of the North China Craton. *Chin. Sci. Bull.* 49, 2495–2502.
- Zhao, Z.P., Zhai, M.G., Wang, K.Y., et al., 1993. *Precambrian Crustal Evolution of Sino-Korean Paraplatform*. Science Press, Beijing 366–384 (in Chinese).
- Zhou, Y.Y., Zhai, M.G., Zhao, T.P., Lan, Z.W., Sun, Q.Y., 2014. Geochronological and

- geochemical constraints on the petrogenesis of the early Paleoproterozoic potassic granite in the Lushan area, southern margin of the North China Craton. *J. Asian Earth Sci.* 94, 190–204.
- Zhou, Y.Y., Zhao, T.P., Zhai, M.G., Gao, J.F., Lan, Z.W., Sun, Q.Y., 2015. Petrogenesis of the 2.1 Ga Lushan garnet-bearing quartz monzonite on the southern margin of the North China Craton and its tectonic implications. *Precambr. Res.* 256, 241–255.
- Zhou, Y.Y., Sun, Q.Y., Zhao, T.P., Diwu, C.R., 2016. The Paleoproterozoic continental evolution in the southern North China Craton: constrains from magmatism and sedimentation. In: Zhai, M.G., Zhao, Y., Zhao, T.P. (Eds.), *Main Tectonic Events and Metallogeny of the North China Craton*. Springer, Singapore, pp. 251–277.
- Zhu, X.Y., Zhai, M.G., Chen, F.K., Lv, B., Wang, W., Peng, P., Hu, B., 2013. ~2.7 Ga crustal growth in the North China Craton: evidence from zircon U-Pb ages and Hf isotopes of the Sushui Complex in the Zhongtiao terrane. *J. Geol.* 121, 239–254.